Astron. Astrophys. 326, 1143–1166 (1997)

ASTRONOMY
AND
ASTROPHYSICS

Observation and modelling of main sequence stellar chromospheres

VI. H_α and Ca II line observations⋆ of M1 dwarfs and comparison with models

E.R. Houdebine[1,2,⋆⋆] **and H.C. Stempels**[2,⋆⋆⋆]

[1] Sterrenkundig Instituut "Anton Pannekoek", University of Amsterdam, Kruislaan 403, 1098 SJ Amsterdam
[2] Solar System Division, ESA Space Science Department, ESTEC Postbus 299, 2200 AG Noordwijk, The Netherlands

Received 29 January 1996 / Accepted 8 June 1997

Abstract. We compare hydrogen and calcium line calculations for dM1 (Teff=3500K) stellar chromospheres with high resolution observations of a selected sample of stars with the same spectral type ($(R-I)_K$=0.875±0.05). We bring evidence that grids of uniform model atmospheres in the plane-parallel and hydrostatic equilibrium approximations can reproduce the average spectral signatures throughout the entire activity range. Observations confirm that when magnetic activity level rises, the Hα line is first weak, then increases in absorption strength, rapidly fills in and eventually goes into emission. We obtain a correlation between the Hα line width and equivalent width that is in good agreement with our model calculations. Simultaneous Hα and Ca II line observations allow to remove the degeneracy in Hα equivalent width for low activity (weak absorption) and intermediate activity stars (filled in profiles). We show that the latter group represents a significant proportion of the stellar population. Within the active stars group, we find an *exclusion zone* in the [0.25Å;-1Å] Hα equivalent width domain, that can be simply explained by the rapid change from the absorption to the emission regimes when the chromospheric pressure increases.

In our sample of 154 stars, covering a large luminosity range, we found no "zero-Hα" stars but instead a minimum (possibly "basal") Hα equivalent width of ∼0.20Å which, with reference to our models, suggests a transition region column mass of log(M)∼-5.5. This implies that for an overwhelming majority of M1 type dwarfs the amount of non-thermal energy input in the chromosphere is much higher than in the Sun, and by reference to acoustic heating calculations, that they are also magnetically much more active (per unit area).

Our observations provide evidence for gradual and important changes in the integrated physical properties of the chromosphere throughout the activity range. For example, the equivalent widths of the H and K line cores are tightly correlated with their ratio, the later decreasing from low activity (∼ 1.50 at -0.2Å) to high activity stars (∼ 1.06 at -15Å). The K lines are also typically 30% broader than the H lines and their widths increase with increasing activity level. This suggests that their optical depths in their region of formation also increase with increasing activity level. Our calcium line calculations reproduce the observed trends.

We confirm a near UV and blue excess in active dMe stars that increases with activity level; in average 0.12 magnitudes in U-B (and up to 0.26 mag.) and 0.03 magnitudes in B-V. This excess is about three times larger than expected from our calculations for a given atmospheric pressure, and together with discrepancies between models and observations for spectral lines, all converge to imply that high pressure plages with a filling factor of about 30% are present on these stars. Low metallicity halo dwarfs in our sample also exhibit a U-B excess, but in the case of single dMe stars an effect of metallicity is excluded.

In our sample, single dMe stars are more luminous than their less active absorption line counterparts. We present an activity-luminosity relationship for the Ca II lines; namely, the Ca II line fluxes rise as the power of 5.4 of the stellar radius. Hence, we expect the stellar magnetic flux to rise approximately as the power of 7.4 of the radius; an important constraint for the dynamo mechanism. Such a correlation is also found with Hα and L_X, the X-ray luminosity. With our present understanding, these correlations are, at least partly, *activity-metallicity relationships*. We emphasize the importance of metallicity on stellar activity as a whole, i.e., metal deficient stars are also activity deficient.

Key words: radiative transfer – stars: activity – stars: chromospheres – stars: late-type – stars: pre-main sequence

1. Introduction

Dynamo theories (e.g. Roberts 1967, Parker 1979, Priest 1982) emphasize the importance of the stellar internal structure on the magnetic field generation, which is itself dependant on the

Send offprint requests to: E.R. Houdebine

⋆ Based on observations collected at Observatoire de Haute Provence and the European Southern Observatory

⋆⋆ e-mail: erh@astro.uva.nl
⋆⋆⋆ e-mail: stempels@strw.LeidenUniv.nl

stellar fondamental parameters: mass, metallicity, angular momentum, age and binarity. Thus far, investigations have focused on the effects of rotation in relatively young stars and rapid rotators, yielding the rotation-activity relationships, and on the evolution of magnetic activity with age (e.g. Simon 1992 for a review on these topics). Hence, our observational description of the magnetic dynamo remains quite incomplete and unclear: the slow rotators are almost absent in the empirical relations and evolutionary effects have not been disentangled from those of rotation. Moreover, the influence of the other stellar parameters, metallicity and mass for instance, has never been assessed.

One must acknowledge that to unravel empirically the properties of the magnetic dynamo, one needs to isolate and study systematically the effects of all stellar parameters. Because the chromosphere is the prime source of radiative cooling for magnetic non-thermal heating (as far as the energy output is concerned, e.g. Houdebine et al. 1996 for a recent evaluation), its spectral signatures, mainly spectral lines, are a natural choice for such an investigation. Chromospheric lines are also easily observed at high spectral resolution and for almost all spectral types from near-UV to near-IR wavelengths.

Numerous studies have been devoted to chromospheric emission lines, but with comparatively little assessment of their direct relation with the dynamo parameters. An essential difficulty arises from the complex relation between spectral line characteristics and the chromospheric physical properties, and consequently the estimate of its total radiative output that provides a measure of non-thermal heating mechanisms (acoustic and magnetic). Major progress has been achieved with simple theoretical arguments (e.g. Fosbury 1973, Ayres 1979) and with detailed NLTE radiation transfer modelling of spectral lines (e.g. Kelch et al. 1979; Giampapa et al. 1982; Cram & Mullan 1985; Cram & Giampapa 1987). But the precise effects of the stellar parameters involved, that in stellar atmosphere studies translate into surface gravity, metallicity or absolute magnitude, still need to be clarified in empirical correlations of magnetic activity indicators (e.g. Wilson & Bappu 1957, Rutten 1986; Schrijver & Rutten 1987; Rutten et al. 1989).

Because of the enormous task if it was solely explored theoretically, there is a great need for new empirical constraints that will focus numerical simulations towards the most important aspects of the problem. In addition, recent grids of model chromospheres for M type dwarfs (e.g. Houdebine & Doyle 1994a,b, 1995; Houdebine et al. 1995, 1996), seem to reproduce major observational trends and suggest that new empirical correlations of great interest may be revealed easily.

In parallel with our effort in modelling stellar outer atmospheres, we undertook an observing program dedicated to compiling a database of stellar atmospheric diagnostics. We gathered high resolution spectroscopic observations of K and M dwarfs from various sites. Here, we present recent such observations for a sample of M1 type dwarfs. This spectral type corresponds to our model calculations in Papers III (Houdebine et al. 1995), IV (Houdebine & Doyle 1995) and V (Houdebine et al. 1996). These data, therefore, allow us to assess the relevance of these models. A preliminary report of this work can be found in Houdebine (1995, 1996ab).

2. Observations and data reduction

The ELODIE spectrograph is a cross-dispersed echelle spectrograph with an original optical design that yields evenly spaced orders on the detector (see Special Issue of "La Lettre de l'OHP", 1995). The spectral coverage is from 3890Å to 6820Å with a resolving power of about 45,000. Extraction and reduction procedures were developed and optimized by Queloz (1994).

The aim of our observations was to collect a selective sample of spectra of stars with identical effective temperatures in order to test our numerical calculations for M1 dwarfs (Papers III and V). Our models used a 3500 K model photosphere that corresponds approximately to the spectral type M1; other authors classified these stars from M0 (Allen 1973) to M2 (Lang 1980). According to the effective temperature determinations by Jones et al. (1994), the above effective temperature corresponds to the infra-red color $(R\text{-}I)_K$=0.843. We selected our target stars according to their R-I color within the range $(R\text{-}I)_K \in$[0.82:0.93]. We preferred this selection criterion because of its high sensitivity to effective temperature, low sensitivity to metallicity (Legget 1992; Buser & Kurucz 1992), and the large number of available measurements.

A total of 155 stars were selected, of which we observed 31. These observations were completed with additional high resolution spectra of the Hα and Ca II H lines obtained at ESO with the Coudé Auxiliary Telescope and the Coudé Echelle Spectrograph (1990 data from Houdebine (1990), 1994 data from Foing, private communication). These data were reduced using the standard procedures. We observed stars that spread over a rather large luminosity range, Mv$\in$[8.95:10.4], and Mv$\in$[8.2:11.1] when including other published data (see Sect. 3). In our data compilation, the measurements are evenly spread in the $(R\text{-}I)_K$ band with an average value of 0.872.

Our data set is not a complete, volume limited stellar sample. We preferably observed the brightest objects which implies a bias towards the more luminous stars. We attempted to cover the whole luminosity range of our sample, but the selection was arbitrary and the distribution as a function of luminosity is not representative of the galactic stellar population. This bias, however, should not affect our correlations providing there is a sufficient sampling density at a given luminosity or activity level.

3. Measurements of spectral lines and radial velocities

We measured the spectral line characteristics (EW, FWHM, self-reversal) for Hα and the Ca II resonance doublet. Equivalent widths are respectively positive and negative for absorption and emission lines. With reference to Fig. 5b, we define for Hα the *central self-reversal* SR and the *relative central depth* RCD as follows;

$$SR = 1 - Ha_3/Ha_2 \quad (1)$$

$$RCD = Ha_3/Ha_1, \quad (2)$$

SR provides a measure of the relative strength of the self-reversal in emission profiles, an interesting diagnostic of high activity chromospheres (Houdebine & Doyle 1994a,b, Papers I and II thereafter), and RCD measures the line core depth relative to the adjacent continuum.

Our measurements were carried out in an homogeneous manner to minimize measurement uncertainties. This is important for the line equivalent widths, which are largely dependant on the determination of the adjacent continuum. Indeed, the numerous narrow photospheric lines make the continuum level uncertain in M dwarfs. For those stars, the situation is quite different from the solar case in the sense that in M dwarfs the Balmer lines are formed entirely in the chromosphere and have no photospheric contribution. Therefore, the correct continuum level is that in the Hα wavelength range including photospheric lines, which are of course masked by the line itself. Hence, in practice, we took the continuum level as given by the average of the continuum plus photospheric lines in the adjacent spectrum on both sides of the line. This should ensure a more relevant comparison with numerical calculations.

We show a sample of our Hα spectra in Fig. 1. Absorption profiles globally become narrower when weaker, whereas emission profiles are quite similar in shape and exhibit strong and extended wings. Such features were predicted by some model chromospheres (e.g. Papers I, II and III) and will be discussed in more detail below.

The equivalent widths of the H and K emission cores (measured from the H1 and K1 points) were calculated with respect to the continuum, respectively at 3950Å and 3975Å. In M1 type stars, the continuum level is approximately the same at these two wavelengths (Robinson et al. 1990). We show a representative sample of the Ca II H line profiles in Fig. 2. The equivalent width of the core emission covers almost two orders of magnitude from the least to the most active stars.

In Tables 1 and 2 we list our measurements for the OHP and ESO observations. Uncertainties are estimates of $\pm 3\sigma$ for all measurements except for the K to H line ratio where it is $\pm\sigma$. Measurements are in parentheses for Gl 815 and Gl 140A because we suspect that a small flare occurred on Gl 815 (red asymmetry), and Gl 140A appears to be a spectroscopic binary with a cooler active component. Also, a larger uncertainty applies to Gl 29.1A and B because the wings of both profiles are blended. As far as McC 169 and McC 69 are concerned, the spectra consistently point to another luminosity class. Note also that the photometric data of both Gl 140A and Gl 867A used in following sections are affected by the contamination from a cooler companion.

We augmented our observations with other data available in the literature: for Hα (Bopp 1987; Byrne et al. 1985; Doyle et al. 1986; Herbst & Miller 1989; Herbst & Layden 1987; Panagi et al. 1991; Pettersen 1989a; Pettersen & Hawley 1989; Robinson et al. 1990; Rutten et al. 1989; Stauffer & Hartmann 1986; Worden et al. 1981) and for the Ca II lines (Giampapa et al. 1981; Robinson et al. 1990). Very few high resolution observations of the Ca II lines are available and most published data were obtained with a narrow band filter (Rutten et al. 1989), which we believe are less accurate but were used in some instances. The latter measurements in the Wilson photometric index S (Vaughan & Preston 1980) were transformed to equivalent widths according to a direct least square fit to the data measured with both methods: $EW = 0.467\ S^{1.215}$.

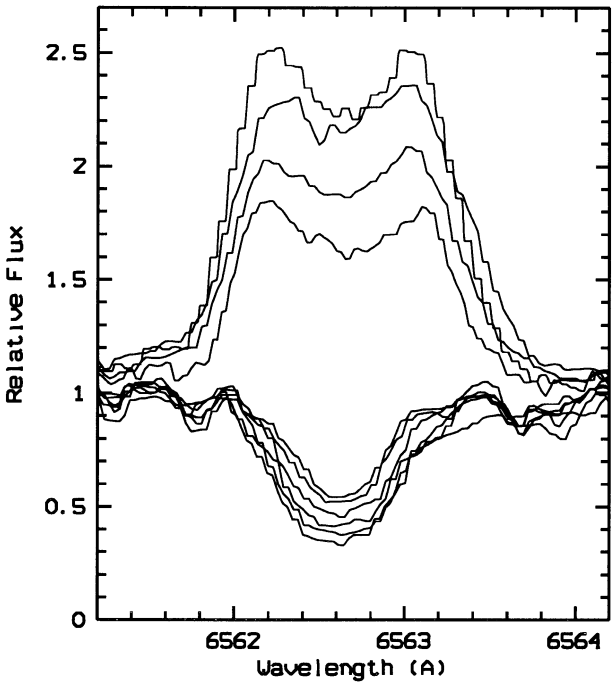

Fig. 1. A sample of the Hα profiles gathered at Observatoire de Haute Provence with the Elodie spectrograph for dM1 stars. We show from top to bottom at line center; Gl 803, St 497, Gl 490A, GJ 1264, Gl 411, Gl 15A, GJ 1010A, GJ 1114, Gl 134 and Gl 275.1. There are significant differences between the absorption profiles, i.e., weaker profiles are narrower. Other features predicted by numerical calculations are the similarities in shape of the emission profiles and the large extension of their wings

Whenever possible, the line parameters were re-measured from the published diagrams for the sake of consistency. We found significant differences with the values given in Panagi et al. (1991) and Robinson et al. (1990). The total number of observations for the equivalent widths are 154 for Hα and 79 for the Ca II lines.

Radial velocities were determined by cross-correlation to a K0 star template. Values are normally accurate to better than 1 km s^{-1}. For most stars, our radial velocities are in good agreement with previous measurements, but we note some important differences for a few stars. For instance, for GL 29.1, GJ 1062, GL 150.1B, and GL 275.1, different velocities are reported in the Hipparcos Input Catalogue (Turon et al. 1992) and the Gliese Catalogue (1991).

Table 1. Hα and Ca II equivalent widths and FWHMs for our program stars observed at Observatoire de Haute Provence (Gl; Gliese 1969, GJ; Gliese & Jahreiss 1988, St; Stephenson, 1986ab, Vy; Vyssotsky, 1943, 1956, 1958). We also give the Hα self-reversal depth (SR), the "relative central depth" (RCD) and the Ca II K to Ca II H line flux ratio. Uncertainties are estimates of $\pm 3\sigma$ for all measurements except for the K to H line ratio where it is $\pm\sigma$. Values of lower significance are in parentheses

Name	V_R $km\ s^{-1}$	Hα EW (Å)	Hα FWHM (Å)	Hα SR	Hα RCD	CaII H EW (Å)	CaII H FWHM (Å)	CaII K EW (Å)	CaII K FWHM (Å)	K/H
Gl 2	-0.67	0.353 0.055	0.715 0.045	-	0.504	-1.24 0.5	(0.268)	-1.9 1.1	(0.30)	1.51 0.14
Vy 354A	-16.30	0.338 0.055	0.724 0.049	-	0.551	-2.0 3.0	0.229	-2.6 2.8	(0.25)	1.26 0.14
Gl 15A	11.68	0.316 0.051	0.626 0.045	-	0.534	-0.26 0.06	0.193	-0.33 0.11	(0.25)	1.29 0.14
GJ 1010A	-64.52	0.371 0.065	0.693 0.067	-	0.470	-0.51 0.41	-	-0.7 1.2	-	1.24 0.5
Gl 29.1	-37.01	-2.41 -	-	-	-	-13.0 8.5	-	-13.4 8.3	-	1.28 0.10
Gl 29.1A	- -	-2.82 0.13	1.385 0.022	(.930).01	2.714	-13.5 7.8	0.391	-13.1 8.1	(0.31)	1.20 0.07
Gl 29.1B	- -	-2.22 0.17	1.341 0.036	(.812).03	2.214	-12.4 9.2	0.330	-13.7 8.4	0.28	1.37 0.12
Gl 49	-6.36	0.254 0.056	0.635 0.10	-	0.597	-2.15 0.28	(0.28)	-2.61 0.52	(0.30)	1.10 0.04
Gl 134	-4.67	0.522 0.085	0.773 0.067	-	0.386	-1.4 1.1	(0.31)	-1.6 1.7	-	1.34 0.22
Gl 140A	19.31	(-0.23) -	(0.73) (0.49)	-	-	(-2.37) 1.7	(0.43)	-2.48 2.3	-	1.30 0.14
GJ 1062	-16.07	3.8 1.0	1.27 0.1	-	0.145	-	-	-	-	-
Gl150.1B	45.95	0.439 0.07	0.760 0.044	-	0.414	-	-	(-1.4)	-	-
Gl 153C	-9.49	1.5 0.5	1.055 0.030	-	0.379	<-0.25	-	<-0.25	-	-
St 497	17.60	-2.37 0.31	1.524 0.040	0.864 0.05	2.231	(-3.4)	(0.37)	(-3.2)	(0.25)	1.17 0.23
Gl 173	-7.04	0.358 0.056	0.661 0.089	-	0.457	-	-	-	-	-
Gl 205	8.25	0.459 0.045	0.618 0.049	-	0.470	-1.13 0.54	(0.29)	-1.5 1.3	(0.34)	1.24 0.18
G192-11A	-0.52	0.249 0.031	0.661 0.054	-	0.619	-2.10 0.33	0.263	-2.71 0.62	0.279	1.31 0.06
Gl 229	4.28	0.497 0.052	0.831 0.045	-	0.410	-	-	-	-	-
Vy 488	8.33	0.413 0.057	0.787 0.062	-	0.474	-1.74 0.78	0.279	-2.0 1.2	(0.30)	1.26 0.10
Gl 275.1	-18.07	0.535 0.065	0.813 0.058	-	0.348	(-0.5)	-	<-0.5	-	-
Gl 289	52.64	0.284 0.072	0.572 0.076	-	0.526	<-0.4	-	-	-	-
Gl 301A	7.54	0.516 0.037	0.840 0.031	-	0.402	<-0.5	-	<-0.5	-	-
GJ 1114	5.98	0.433 0.057	0.706 0.098	-	0.444	-	-	-	-	-
Gl 411	-84.95	0.260 0.068	0.572 0.089	-	0.553	-0.138 0.02	0.174	-0.22 0.06	(0.20)	1.58 0.18
St 928	31.21	0.482 0.057	0.760 0.049	-	0.381	-0.82 0.73	-	-1.0 1.9	-	1.19 0.29
Gl 450	0.02	0.349 0.055	0.688 0.027	-	0.493	-0.88 0.25	-	-1.35 0.5	-	1.45 0.17
Gl 490A	6.75	-1.82 0.28	1.461 0.022	0.828.006	1.942	-4.9 2.0	0.272	-6.2 3.2	0.313	1.32 0.06
Gl 767A	-4.60	0.422 0.054	0.787 0.045	-	0.474	-	-	-	-	-
Gl 815AB	-46.96	(-2.27) 0.30	(1.47) -	(0.782) 0.01	2.111	(-5.7) 7.0	0.265	(-7.2)	0.277	1.17 0.08
Gl 867AB	-9.67	-2.32 0.36	1.37 0.063	0.923 0.01	2.509	>-3.2	(0.31)	>-2.6	-	-
Gl 880	-27.83	0.465 0.065	0.751 0.054	-	0.391	-0.83 0.7	(0.28)	-1.2 1.5	(0.27)	1.49 0.34
Gl 908	-71.70	0.383 0.064	0.657 0.036	-	0.452	<-0.21	-	(-0.44)	-	-

4. New series of model atmospheres

The grids of model atmospheres presented in Paper III do not sample densely enough the whole activity range for comparison with the data presented below, especially in the intermediate activity domain. Based on this previous work and its comparison with the present data, we designed an improved grid of models (Fig. 3) that includes the following new constraints:

- The temperature minimum diminishes with the transition region column mass (M_{TR}) as T_{min} = 40.0 $log(M_{TR})$ + 3350 K.
- The extent of the "temperature break zone" (see Papers I and II) diminishes gradually with the transition region column mass.

Hereafter, our models are referred to as III-1 to III-30, with the transition region column mass taking the following values: logM=-3.0, -3.25, -3.5, -3.7, -3.8,..., -4.0, -4.05,..., -4.7, -4.8,..., -5.2, -5.5, -5.7, -6.0, -6.5. Microturbulence is as described in Paper III.

We performed the calculations for both hydrogen and calcium with the NLTE radiation transfer code MULTI, version 2.0 (Carlsson 1992), and with two approximations for the Ly$_\alpha$ and the Ca II H & K lines: complete frequency redistribution (CRD) and partial frequency redistribution (PRD, Uitenbroek 1989ab). All other spectral lines were treated in complete redistribution.

For hydrogen, we used a 15 level + continuum model atom with 27 b-b and 7 b-f transitions treated in detail. Spectral line calculations are as described in Houdebine & Panagi (1990), except for the van der Waals broadening that was included later. We assume Voigt profiles that include natural, Doppler (temperature and micro-turbulence), Stark (Sutton 1978), van der Waals (Derrider & van Rensbergen 1976), and resonance (Schaifers & Voigt 1982) broadening mechanisms. Here, we used two different sets of collisional excitation and ionisation rates: (i) Giovanardi et al. (1987), Giovanardi & Palla (1989), Seaton (1960) and Mihalas (1967) that were used previously in this series of papers, (ii) Vriens & Smeets (1980) and Janev et al. (1987) (coded by M.J. Stift, private communication). Discrepancies in the Giovanardi et al. data were noted by Chang et al. (1991) who also discussed the relevance of various sources of collisional excitation rates. There remains a large uncertainty in hydrogen collision cross-sections that produce significant effects on theoretical line profiles.

For calcium, the model atom is the same as described in Houdebine (1990) and Doyle et al. (1994). It includes 14 levels (Ca I/8, Ca II/5, Ca III/1), 11 b-b and 13 b-f lines treated

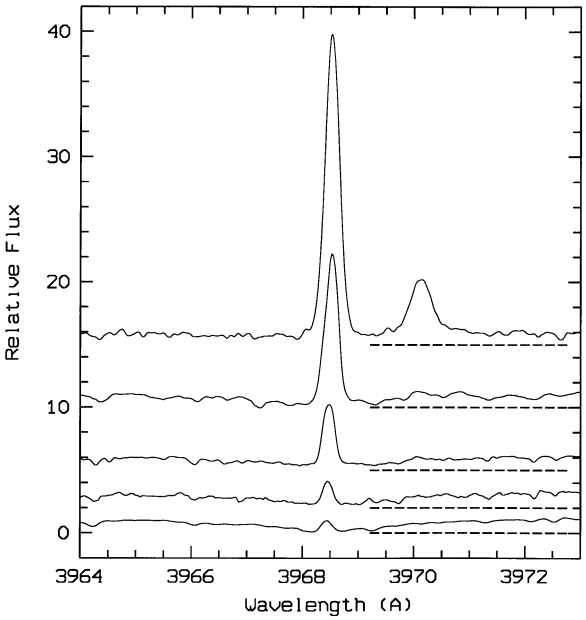

Fig. 2. A sample of the CaII H line profiles with decreasing core emission from top to bottom. The core equivalent width covers almost two orders of magnitude from -0.14Å to -7.5Å. From the top; AU Mic (-7.5Å), Gl 49 (-2.2Å), Gl 887 (-0.90Å), Gl 15A (-0.26Å) and Gl 411 (-0.14Å). The spectra are on the same scale but were arbitrarily shifted along the ordinate axis for better clarity. Note also the filling in of the photospheric wings and the appearance of the H_ϵ line when CaII H becomes of the order of -1.0Å (Gl 887)

Table 2. Same measurements as in Table 1 for the ESO-CES 1990 and 1994 observations

Name	Hα EW (Å)	Hα FWHM (Å)	Hα SR	Hα RCD	CaII H EW (Å)	CaII H FWHM (Å)
			ESO 1990			
Gl 803	-2.71 0.5	1.447 0.03	0.827 0.01	2.324	-7.52 1.5	0.285 0.005
Gl 887	-	-	-	-	-0.903 0.01	0.246 0.005
Gl 908	0.360 0.07	0.665 0.04	-	0.489	-0.204 0.05	0.164 0.013
			ESO 1994			
Gl 85	0.20 0.05	(0.45)	-	0.472	-	-
Gl 271	0.474 0.01	0.78 0.12	-	0.419	-	-
St 1806	0.22 0.05	(0.59)	-	0.591	-	-
Gl 803	-1.99 0.55	1.459 0.043	0.864 0.08	1.984	-6.1 0.1	0.291 0.002
Gl 821	0.25 0.05	0.65 0.2	-	0.563	-	-
Gl 832	0.410 0.05	0.684 0.066	-	0.431	-0.2 0.1	0.25 0.03
Gl 836.9B	0.601 0.024	0.900 0.04	-	0.336	-	-
GJ 1264	-1.05 0.20	1.43 0.07	0.742 0.03	1.621	-5.2 0.1	0.27 0.03
Gl 867A	-2.13 0.43	(1.53) 0.06	-	2.412	-5.0 0.1	0.259 0.001
Gl 867B	-3.52 0.8	1.30 0.06	-	3.607	-	-
Gl 887	-	-	-	-	-1.0 0.1	0.261 0.002

in detail. Line profiles are calculated as above and include natural, Doppler, van der Waals and Stark (according to Mihalas 1978) broadening mechanisms. Collisional rates are given in Houdebine (1990).

Below, we compare three sets of calculations: (a) H I collisional data set (i) with all lines in CRD, (b) H I collisional data set (ii) with all lines in CRD, and (c) H I collisional data set (ii) with Ly_α and Ca II H & K lines in PRD. Calcium lines where calculated after the hydrogen calculations that included the relevant electron density corrections assuming hydrostatic equilibrium.

Differences in electron densities when assuming Ly_α in CRD and PRD (runs (a) and (b)) are illustrated in Fig. 3 (lower panel). Since frequency redistribution due to collisions with electrons is larger at high densities, the effects of PRD are negligible in our high pressure models (at chromospheric levels), but become increasingly important for low pressure models. However, the effects on the Balmer lines and particularly H_α remain relatively small (typically below 50mÅ) and can be neglected in the emission domain. They are proportionally the largest for intermediate activity profiles (emission wings and absorption core) when the equivalent width passes through a null value (see Paper III and below), but in terms of transition region column mass versus H_α EW, the effects are very small. We conclude that the CRD approximation is appropriate for modelling hydrogen lines (others than the Lyman series) in M dwarf atmospheres.

We found that the largest effects on hydrogen and calcium line calculations arise from using different hydrogen collisional cross-sections rather than the CRD approximation. Stark broadening is also an essential parameter for the Balmer series. The PRD approximation has the largest effect on the wings of the emission core of the Ca II H & K lines, i.e. wings are weaker when treated in PRD, a well known effect of partial redistribution. The inner wing flux is generally larger under the CRD assumption, typically by a factor of two. However, for the lowest pressure model atmospheres, we found the opposite effect; the emission is larger in PRD because the K1 fluxes are smaller but the line core flux is unchanged, hence the flux integration between the K1 points is larger.

5. Spectral line characteristics

In this section, we analyse and cross-correlate H_α and Ca II line spectral diagnostics, and compare with our series of models. We assess the relevance of our approach and comment on possible causes for the discrepancies between observations and models.

5.1. H_α: FWHM versus equivalent width

5.1.1. Observations

We found that the H_α FWHM correlates with its equivalent width as shown in Fig. 4a. According to our calculations (see also references therein), when activity level increases, the equivalent width first increases when in absorption (left panel), attains a maximum, then the line fills in, and eventually it goes into emission (Fig. 4b).

For absorption profiles, the observed FWHM increases steadily with the EW and the data are more or less evenly scattered within a band of approximately 0.15Å width in the direction parallel to the Y axis. This is of the order of the estimated 3σ error, and one could be tempted to interpret the scatter as due to measurement uncertainties. However, our measurements should then show less scatter than other data (which also include narrow band photometry), and this is not the case. Hence

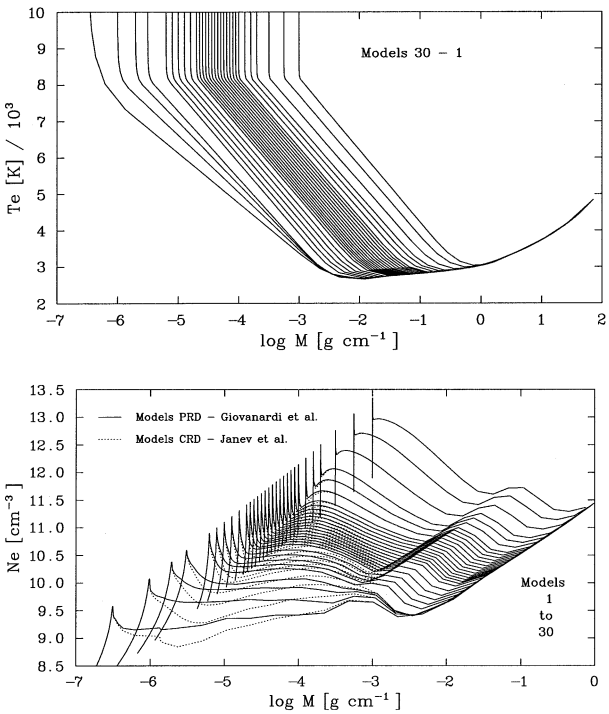

Fig. 3. Grid of model chromospheres for M1 dwarfs. Top panel, electron temperature as a function of column density. Lower panel, electron density as a function of column density (assuming hydrostatic equilibrium) for Ly_α calculated with two approximations: complete redistribution (CRD) and partial redistribution (PRD). These new models can reproduce several characteristics of the H_α and CaII lines as described in subsequent figures

we looked for possible systematic effects, such as from the effective temperature.

We divided the data-set into three narrower bands in R-I ([0.81:0.86],]0.86:0.90] and]0.90:0.94]) so as to look for a possible effective temperature effect on the width of the correlation. We found that the measures in each sub-band contribute equally to the global scatter.

We also separated our data set into three subsets according to the absolute visual magnitude Mv (Fig. 4a); Mv$\geq$10.2; 9.6$\leq$Mv$<$10.2 and Mv$<$9.6. We found that active stars are brightest, and in the H_α absorption domain the Hα equivalent width decreases with luminosity. The above domains coincide roughly with the following Hα equivalent widths: EW$>$ 0.44 or emission, 0.35$\leq$EW$\leq$0.44, EW$<$0.35. However, neither the color nor the luminosity seem to play a role on the scatter in this correlation. This suggests that other parameters are affecting the shape and strength of the H_α line profile. Magnetic activity by way of surface inhomogeneities can be important. This means that even for very low activity stars (EW$\sim$0.25Å), sizable surface inhomogeneities and magnetic fields are present. This argument finds strong support in the observed variability of the profiles for a given star. For instance, Gl 411 was observed to have an EW in the range 0.26-0.40mÅ, Gl 2 in 0.35-0.45mÅ and Gl 15A in 0.28-0.33mÅ. Variability in H_α emission stars is also remarkable and we call attention to a 0.72mÅ change for AU Mic (-1.99 to -2.71Å).

5.1.2. Comparison with models

Models are compared with observations in Fig. 4b. Our theoretical profiles were convolved with a 0.15Å FWHM Gaussian profile to account for the limited resolving power (45,000). Models fall within the range of observations, but our new calculations show, unlike our previous models (Paper II), that after attaining a maximum equivalent width and FWHM, the latter actually decreases significantly before the profile goes into emission. Therefore, there is almost a degeneracy in this diagram between low activity (0.2Å to $\sim$0.45Å) and filled-in "intermediate activity profiles" (0.52Å to 0.0Å before the emission regime).

We had to refer to the Ca II lines to remove this degeneracy in our interpretation of the data (see Sect. 5.5). Based on these measurements, the data show that there is a lower, possibly basal, limit of $\sim$0.20Å for the least active stars and that "zero-H_α" M1 stars most probably do not exist (considering the activity-luminosity relation, Sect. 7). This minimum basal equivalent width yields a minimum transition region pressure and can be useful for the modelling of acoustic heating. At the other extreme, the maximum equivalent width appears to be $\sim$0.52Å when one excludes the singular case of Gl275.1 (0.535Å) and corresponds to the lower limit (upper limit in EW) of the intermediate activity domain.

The observed minimal equivalent width indicates that the minimum column mass in the transition region is, with reference to our models, about 3 $10^{-6} gcm^{-2}$ ($logM = -5.5$), which is very close to the value obtained for the quiescent average Sun (Vernazza et al. 1981) or for acoustically heated basal chromospheres of M dwarfs (Mullan & Cheng 1993). This shows that at the transition region level, the non-thermal heating rate is of the order of or larger than that of the quiescent Sun (per unit area). In other words, *all M1 dwarfs are at least as active as the Sun, which by this standard is a very low activity star*.

A few stars are convincingly observed in the intermediate activity domain where the H_α profiles are *filled in* (see Sect. 5.5). We show in Fig. 5 (left panel) an example of such a profile (Gl 49) together with a low activity profile (Gl 289) of similar equivalent width but with Ca II lines an order of magnitude weaker (Table 1). The former exhibits a filled in core, a wider core absorption and some wing emission. These features are weak but real: we compared Gl 49 with G 192-11A which have very close "intermediate activity" levels, and they show a perfect match of their profiles. The same also applies to the profiles of Gl 289 and Gl 411, two low activity stars, but the comparison with the two extreme activity levels show a significant difference as illustrated in Fig. 5. It therefore appears that a number of dM stars are in fact fairly active (the "intermediate activity" stars), with activity levels being in continuity with those of dMe stars (see also Sect. 7).

We plot in Fig. 5 (right panel) the numerical profiles corresponding to these intermediate activity stars. They show features in accordance with observations, but the profile difference does

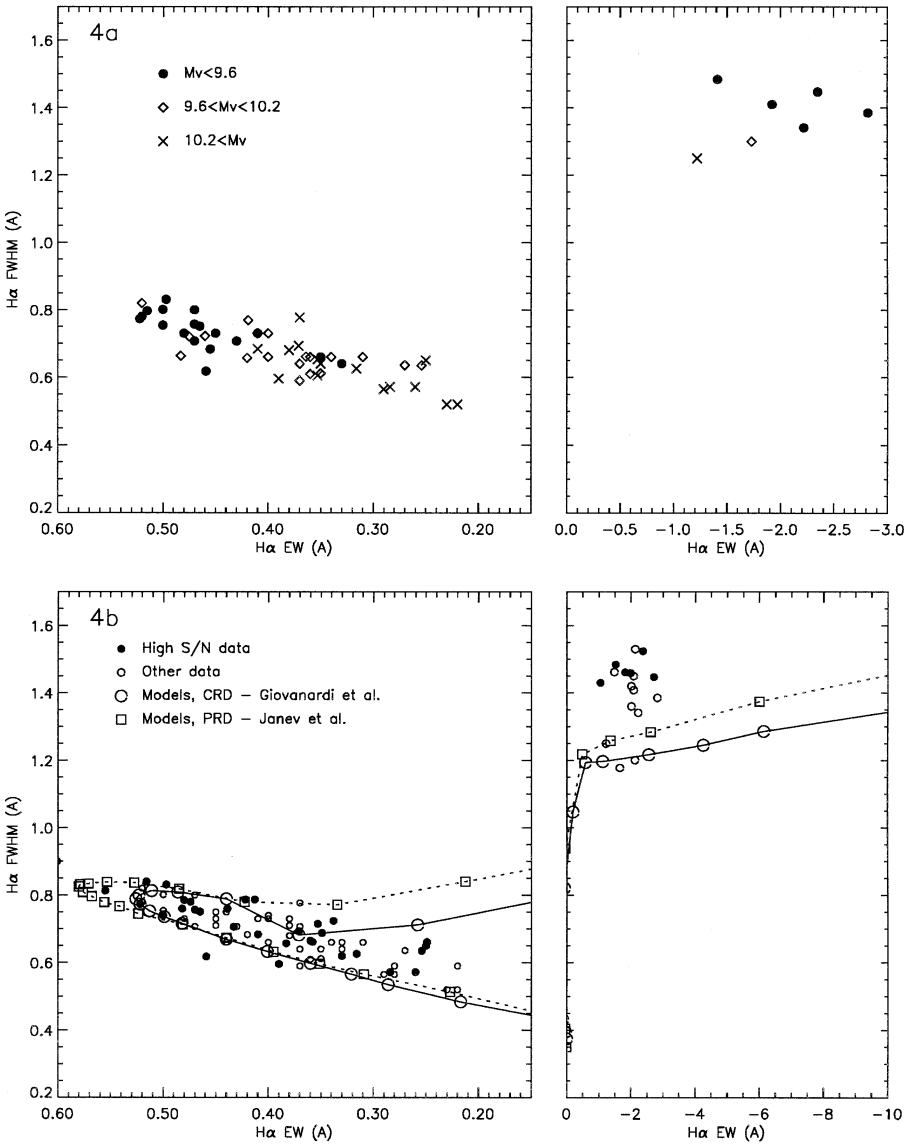

Fig. 4a and b. In **a** we plot the H_α FWHM against its equivalent width: the left and right panels are respectively for absorption and emission profiles. We separated the data into three different luminosity intervals: Mv$\geq$10.2 (crosses), 9.6$\leq$Mv$<$10.2 (diamonds) and Mv$<$9.6 (filled circles). We note that the absorption profiles broaden when they strengthen, and that surface magnetic activity increases with luminosity (see text). In **b** we plot the same data augmented with stars with unknown parallax, but we separated high quality data (filled circles) from the other data. To help interpret these data, we superimposed our models shown as circles and squares connected by solid and dashed lines. When the activity level increases, the equivalent width first increases (absorption, left panel), then reaches a maximum, decreases as the profile "fills in", and eventually goes into emission (right panel). While there is a satisfying agreement between observations and models, there is a significant difference between the two sets of calculations that emphasizes the effects of collisional rates for hydrogen (see text)

not match well the observed difference spectrum. Models tend to yield a core filling in that is too strong and wing emission that is too close to the core. This may indicate that the turbulence in our models has been underestimated at intermediate activity levels, and that it increases with activity.

As we shall see in Sect. 5.5, *in our sample* (when Ca II line measurements are available) the stars spread along the activity range in the H_α absorption domain, but there seem to be fewer intermediate activity stars than low activity stars.

The calculation sets (a) and (c) (see previous Sect.) are compared in Fig. 4b. In the emission regime, the CRD and PRD approximations yield almost identical results and differences are entirely due to the different sets of collisional rates. In the absorption domain, the PRD approximation tends to yield slightly broader profiles near maximum equivalent width, but again, the main effect is due to the changes in the collisional rates.

There is good agreement between observations and model series (a) for the maximum absorption equivalent width and also for the overall trend. Models delineate the envelope for observations, which can be interpreted as an indication that in most cases we do not observe profiles that correspond to a unique model atmosphere, but instead combinations of model atmospheres as a result of surface inhomogeneities. Series (b) models yield a maximum equivalent width that is larger than observed and therefore indicates that a series of model atmospheres with a lower temperature at the base of the transition region may give better results for this set of parameters.

There seems to be an *"exclusion zone"* near the transition between the absorption and emission regimes. In the 0.25Å$>$EW$>$-1Å domain, no stars are observed, which can be explained simply by the very rapid changeover from the absorption to the emission domains (Paper III). It is therefore unlikely that stars with a weak net emission such as Gl 900

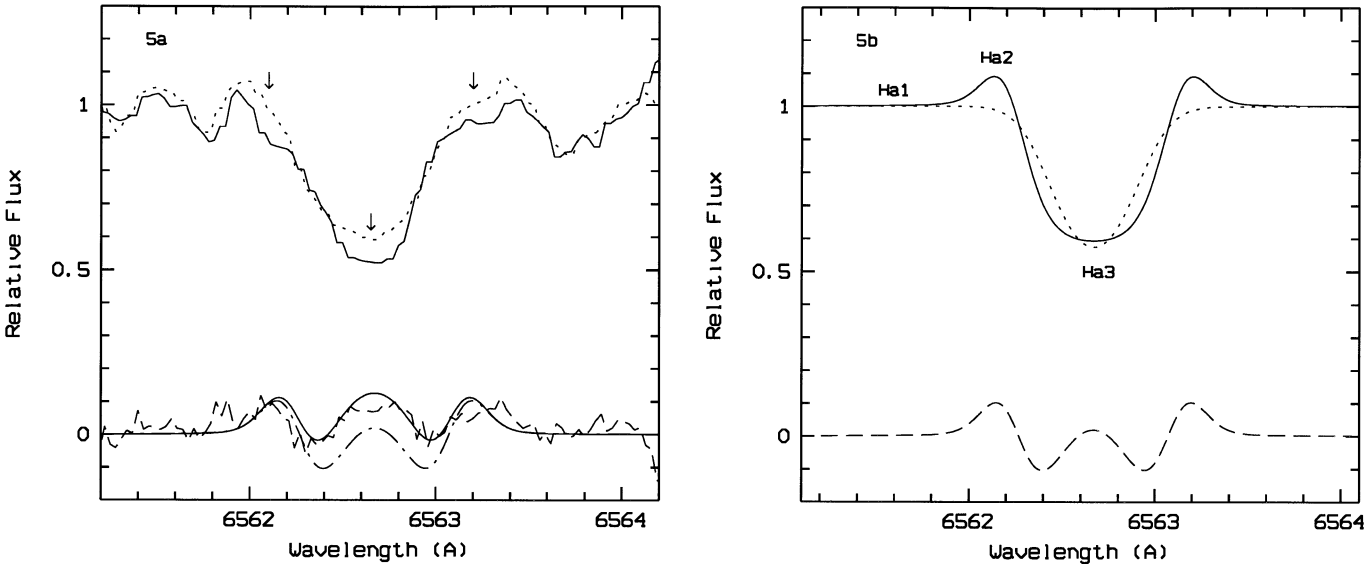

Fig. 5a and b. In the left diagram **a** we plot a "low activity" and an "intermediate activity" profile with similar equivalent widths (filled in; Gl 49, dotted line, and low-activity; Gl 289, continuous line) and their difference (dashed profile). In intermediate activity profiles, emission develops in the line wings and core giving a difference profile with three humps (see text). In the right panel **b** we compare two relevant theoretical profiles (models III/10 (continuous) and III/27 (dotted)) and also show their difference. We also plot this difference profile in the left panel together with another theoretical difference profile (III/11-III/25) so as to compare with the observed difference profile. The models reproduce the three humps but yield a wing emission that is too close to the line core

or Gl 907.1 (Robinson et al. 1990) are observed. Globally, the models, though very simple, are fairly successful in reproducing both the gradient and the average line width for a given equivalent width in the absorption domain.

As far as emission profiles are concerned, our measurements show that the observed FWHM varies only within a 0.15Å wide band for high signal to noise ratio data, and over a factor of 2.7 change in equivalent width (-1.05 to -2.71Å). When we include other sources, the scatter domain is larger (1.18Å to 1.55Å), probably because of measurement errors, fitting approximations (Stauffer & Hartmann 1986), or because the H_α wing contribution to the adjacent continuum (Fig. 1) was not taken into account.

Models of series (a) and (b) give values on average about 0.25Å and 0.15Å, respectively, below the observations (Fig. 4b). According to the calculations in Paper I, rotational broadening, in the range 4-10$km\ s^{-1}$ for all our dMe target stars (Houdebine et al., in prep.), could account only for 0.05Å additional broadening to the line profile. According to the same study, turbulence also has little effect on the line width, unless it is rather large and beyond the upper limit found by Giampapa et al. (1982). Hence, as we also concluded in our detailed modelling of AU Mic (Paper II), the significant discrepancy between the models and observations implies the presence of high pressure plages. FWHM in the 1.35-1.55Å range are produced by models (series (c)) with column masses at the transition region in the range logM∈[-3.20:-3.55], which would imply plage filling factors in the range 15%-40%. A similar result was obtained in our Paper II, where the modelling of AU Mic (dM1e) required a plage filling factor of 30%. On the other hand, the nearly constant width in the emission domain suggests that the plage filling factor varies from star to star rather than the plage pressure, and that turbulence, if significant, does not increase substantially.

The variety of observed Hα profiles throughout the entire activity range, however, cannot be reproduced by simple combinations of quiescent and plage type profiles with different degrees of surface coverage. For example, we cannot obtain the weak "low-activity profiles" with a combination of a strong absorption and an emission profile without obtaining emission in the inner wings. Besides, the simultaneous Calcium line observations point to important changes in the chromospheric integrated properties. Therefore, along the activity domain, large changes take place in the integrated physical properties of the chromosphere, probably both in plages and in "quiescent regions" (through X-ray backwarming for instance, Cram & Woods 1982). Our observations also consistently point to some degree of surface inhomogeneity (variety and variability of profiles) at all activity levels.

5.2. H_α relative central depth versus FWHM

As an attempt to alleviate the near-degeneracy of intermediate activity ("filled in") and "low activity" profiles in Fig. 4, we used another spectral line characteristic; the Hα relative central depth (RCD thereafter), defined as the ratio of the flux at line center to the continuum flux. Indeed, besides the near wings that are difficult to measure, the greatest difference between the above-mentioned profiles occurs at line center and not in the equivalent widths (Fig. 5).

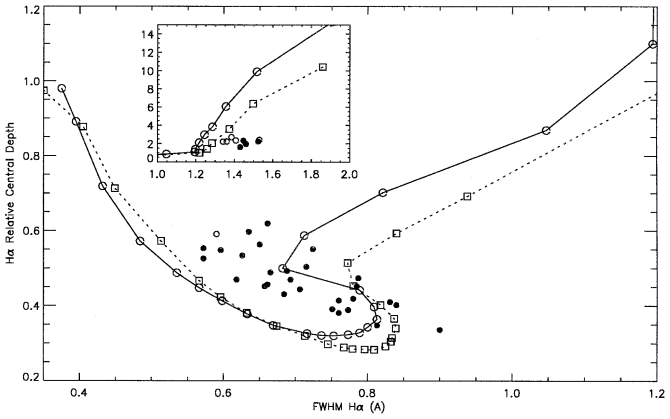

Fig. 6. We plot the Hα Relative Central Depth, i.e., the line center to continuum flux ratio, as a function of the FWHM (symbols have the same meaning as in Fig. 4b). This curve characterizes better the line profile shape than the EW vs. FWHM curve in Fig. 4. Comparison with the data shows that theoretical profiles are too deep for a given width and that an important factor, likely surface inhomogeneities, is responsible for the variety in the observed profile shapes.

We plot in Fig. 6 the RCD versus the FWHM for our observations and the models. As shown by the models, the line profiles are much better differentiated in this diagram. On the contrary, the observations are evenly scattered and are not yet conclusive as for significantly different populations. They show that the profiles are quite varied in shapes in spite of meaningful differences between them at the extremes of the activity domain. The reason for such a variety is not clear, but we suspect that surface inhomogeneities or surface gravity plays a significant role. Rotation can be disregarded because it is too small (Houdebine et al. in prep.).

The models somewhat disagree with observations: although they form an envelope that includes most stars, the data delineate a lower envelope that lies significantly above the models. In other words, the theoretical profiles are too deep for a given width.

There is also some disagreement when Hα is in emission: the profiles are too narrow for a given central flux by $\sim$0.20Å, about the same amount as for the FWHM vs. EW data (Fig. 4). As noted in the previous section, rotation and turbulence are too small to resolve this difference and we reach a consistent conclusion that plages are important with a filling factor of the order of 30%, i.e., the line fluxes are a factor of $\sim$3 too large for a given line width. Nevertheless, numerical approximations such as in our continuum calculations may yield important revisions to such values.

5.3. H_α: central reversal versus equivalent width

For Hα, the measure of the self-reversal (SR, the ratio of the average Ha_2 fluxes to the Ha_3 flux) turns out to be an interesting pressure diagnostic for dMe chromospheres (see Papers I, II & III). This ratio varies continuously from the true emission profiles to filled-in profiles and absorption profiles: SR$\rightarrow$0 when the central reversal disappears at very high activity levels (not observed) and SR$\rightarrow$RCD for absorption profiles when wing emission disappears. We plot SR as a function of EW in Fig. 7. Our theoretical line profiles are convolved with the instrumental profile, but no rotational broadening was taken into account. We added to our own data observations of Gl 900 ((R-I)$_K$=0.81) and Gl 907.1 ((R-I)$_K$=0.77) obtained by Robinson et al. (1990). Although those stars do not have exactly the same spectral types as those in our sample, profiles of this type (as well as those in emission) are believed to be sufficiently similar over a reasonable spectral range (Paper I) for this prospective comparison.

Observations of the SR values spread over two orders of magnitude. We fitted these data with a power law function (Fig. 7 & Table 3). The models agree rather well with the observations down to an SR value of 1 (intermediate activity domain). They are typically a factor of 1.5 above observations in this range, pointing again to the overestimated central depth of the profiles. Model departures from the observations are increasingly large when H_α emission increases. They reach a factor of 4 for typical H_α emission strengths.

Typical observed SR values are of the order of 0.15 for dMe stars, but the smallest value obtained with our models (series (c)) is 0.23. Hence, surface inhomogeneities are insufficient to reproduce observations as this would imply transition region pressures in plages larger than that of our model atmospheres and somewhat in contradiction with the other H_α and Ca II line parameters. Clearly, our calculations in Paper I show that the relative depth of the self-reversal is quite sensitive to rotation. In the range investigated, turbulence did not seem as significant, but we do expect a larger effect on the emission edges (H2 points, Fig. 5) than on the FWHM. Rotation in the 4-10 km s^{-1} range (Houdebine et al. in prep.) decreases the self-reversal by a factor of $\sim$1.5: this yields a minimum model value of 0.15, in agreement with observations and consistent with our findings on the FWHM vs. EW and RCD vs. FWHM correlations. Thus, once again one needs to include plages with a high transition region column mass but with a filling factor of the order of 10%. This filling factor is somewhat smaller than that required to reproduce the FWHM vs. EW and RCD vs. FWHM data. We propose that in the upper chromosphere turbulent motions are high enough to smooth out the H2 features. It is interesting to note that in all of our H_α spectra the H2R flux is systematically larger than the H2B flux (Fig. 1), which is evidence for systematic and relatively large velocity fields in the upper chromosphere. In addition, the difference between models and observations is larger for the SR than the FWHM. Since these two diagnostics are related to the upper and central layers of formation of the H_α line respectively, it may be that turbulence increases with height.

5.4. Ca II lines

M1 stars are faint in the blue and observations of the Ca II resonance doublet are difficult and scarce. We obtained a signal-to-noise ratio typically less than 20 in the continuum adjacent to those lines in our spectra. The most accurate measurements

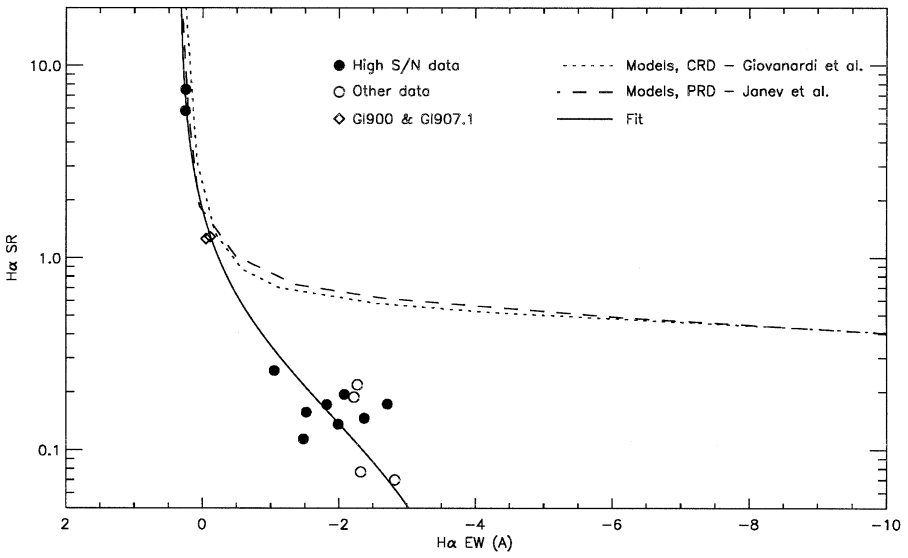

Fig. 7. Hα self-reversal (only for profiles in emission or showing a wing emission) as a function of the equivalent width. To our M1 star sample (R-I=[0.82:0.93]) we added the remarkable profiles of Gl 900 (R-I=0.81) and Gl 907.1 (R-I=0.77) observed by Robinson et al. (1990). The fit to the data is very close to theoretical curves down to SR=1 (intermediate activity), whereas for smaller values (high activity) differences are large. If turbulence is as low as claimed by Giampapa et al. (1982), then surface inhomogeneities must be responsible for this difference (e.g. Paper II for the particular case of AD Leo)

are for the equivalent widths, whereas the line widths could be determined with a sufficient precision only in a few cases.

We show in Fig. 8 the Ca II K versus H equivalent widths for the emission line core measured between the H1 or K1 points. These data describe a tight linear correlation that can be fitted by a power law;

$$EW_{CaIIK} = 1.31(EW_{CaIIH})^{0.921}. \quad (3)$$

The correlation is quite good over almost two orders of magnitude and indicates that the conditions of the Ca II line formation change with their EW (a good indicator of magnetic activity level). It shows that the line ratio tends towards unity at high activity levels, i.e., the line formation becomes *effectively optically thick* (flux ratio given by the Planck function, i.e. $\simeq$1), whereas at low activity levels the ratio tends towards 2, i.e., the line formation tends to be *effectively optically thin* (flux ratio given by the oscillator strength ratio).

The empirical fit to the data (Eq. (3)) predicts an effectively thin regime for an equivalent width greater than -5mÅ, which is 40 times less than the currently detected minimum emission. Hence, we believe that, unlike in evolved or hotter stars (Judge 1990), the exact optically thin case will never be reached for M1 dwarfs, even for the lowest activity stars.

The smallest average H & K equivalent width observed for a dM1 star is -0.179Å for Gl 411. This corresponds to a transition region column mass $logM = -4.85$ (according to series (b)), somewhat larger than the value inferred from the minimum Hα equivalent width; $logM = -5.5$. Those values are respectively larger than and close to that of the solar quiescent atmosphere and further emphasize that inactive M1 dwarfs as proposed for instance by Doyle et al. (1994) most probably do not exist. We may further speculate that, (i) because of the relatively high incidence of H_α emission and slow decline in coronal X-ray flux among later M dwarfs (e.g. Barbera et al. 1993), and (ii) because stellar parameters for late K and M dwarfs are similar, late K and M dwarfs have (on average) much higher pressure

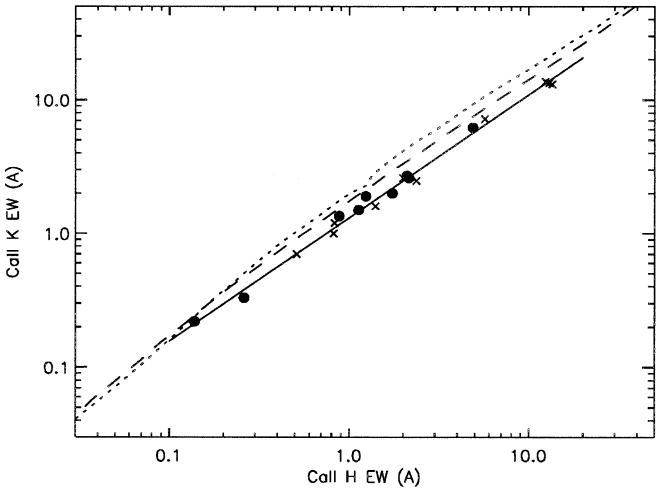

Fig. 8. CaII K line equivalent width versus CaII H line equivalent width. Circles and crosses are respectively for high and low accuracy measurements. Continuous and dashed or dotted lines are, respectively, the least square fit and our models (same description as Fig. 7). The data show a good correlation with a 0.921 slope that is evidence for changing conditions in the line formation throughout the activity range, namely the CaII lines tend to be effectively optically thick at high activity levels whereas they tend to be effectively optically thin at low activity levels

chromospheres than the Sun and there is no "zero H_α" (inactive) star in this group.

Unlike the H_α line, there is no clear lower limit for the calcium equivalent widths, perhaps because of the scarcity of our data. Different metal abundances probably play a large role because, unlike H I lines, they directly affect the Ca II line formation (the H I lines may also be affected, but indirectly and for very low metallicities, see Sect. 8). Radiation-transfer-induced variations in the K to H line ratio from the optically thin to optically thick cases would induce a 0.3 excursion in Fig. 8 with respect to the correlation, whereas the actual maximum departure is only 0.08 (factor of 1.2). Hence these data show that *there*

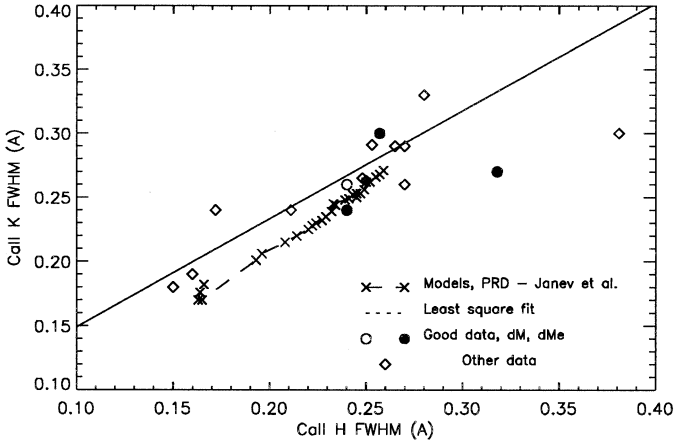

Fig. 9. CaII K line width as a function of CaII H line width. The line widths increase simultaneously and monotonically, but the K line remains about 30% broader because the optical depth in this line is a factor of two larger. Models agree with observations in this diagram, but Fig. 10 shows that except for intermediate activity stars, the width departs significantly from the empirical corelation

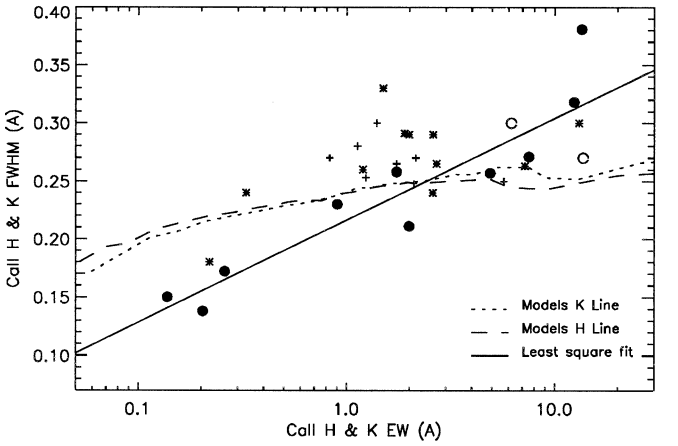

Fig. 10. CaII line FWHMs as a function of their equivalent widths. Circles and other symbols are, respectively, for the best and least accurate measurements (•, + and ○, ∗ are, respectively, for the K and H lines). The line widths increase twofold over the equivalent width domain. Model values rise much more slowly and even level off for large equivalent widths

is a great homogeneity in the spatially integrated characteristics of the Ca II lines, and hence in the spatially integrated properties of the lower chromosphere to which all stars obey within measurement errors. They also show that these properties vary continuously throughout the activity domain.

We superimpose a plot of our calculations on the data in Fig. 8. The core emission for our models was also measured between the H1 and K1 points and the equivalent widths were calculated with respect to the continuum adjacent to the K line.

Model line ratios (Series (c)) monotonically diminish from 1.83 for a K line equivalent width of -0.4Å to 1.28 at -51Å, and they also diminish towards smaller equivalent widths; 1.64 for an equivalent width of -0.11. We also obtained line ratios larger than the ratio of the oscillator strengths for a few models in Series (a). This is in principle impossible and is evidence that the flux measured between the H1 and K1 points does not accurately represent the chromospheric radiative losses.

The observed trend is globally reproduced throughout most of the activity range, but models generally fail to give the observed ratio for a given equivalent width. The reasons for this are unclear because a number of parameters may be at work; turbulence, temperature structure, surface inhomogeneities, calcium abundance, surface gravity and theoretical approximations. Detailed models of the line profiles for a range of stars will be necessary to specify in more detail the lower chromosphere.

In general our theoretical profiles show a weak self-reversal in the core emission profile that was not present in the observed profiles. Although higher resolution and signal-to-noise ratio observations are required to confirm this. We plot in Fig. 9 the correlation between the H and K line full width half maximum for observations and models. We plot the intrinsic line widths determined by deconvolving the instrumental point spread function from the observed widths assuming Gaussian profiles (0.088Å FWHM at 3950Å for the instrumental profile): $\mathrm{FWHM} \simeq (\mathrm{FWHM}^2_{obs} - \mathrm{FWHM}^2_{PSF})^{1/2}$. We convolved the theoretical profiles with the instrumental profile, and then measured the FWHM. We then recomputed the FWHM after proceeding to the inverse operation and assuming Gaussian profiles for both the line and instrumental profiles. This procedure ensures a better comparison between models and data.

There is a large scatter due to measurement uncertainties, but on average the Ca II K line width is larger by about 0.3Å, i.e. ∼30%. Models show the same trend but they do not cover the whole range of observations. They succeed in reproducing the smallest widths but not the larger values. In addition, one can see in Fig. 10, which shows the FWHM as a function of the equivalent width, that the gradients for the theoretical curves are much shallower than that of the empirical fit to the data. Stellar rotation was not taken into account but is in the range 1-10 km s^{-1} (Houdebine et al. in prep.), and therefore could explain most of the observed difference for the active stars. Conversely, the important discrepancy for the smallest equivalent widths cannot be accounted for by rotation because rotational broadening is too small for low activity stars. It also is unlikely that it could be attributed to turbulence because; (i) broadening due to turbulence in our models is small (< 2 km s^{-1}) and decreases with the transition region pressure (lines are formed deeper in the chromosphere where turbulence decreases) and, (ii) turbulence is not the main contributor to the widths. Radiation damping controls the line widths. For this reason, the very small widths observed for the low metallicity stars only (Sect. 7) point to an important effect of the calcium abundance on the line formation. This discrepancy between models and observations instead indicates that the abundances used for low-activity models are inadequate (solar abundances were assumed for all our models).

In Fig. 10, the correlation seems linear and the line widths double when the line flux has increased by two orders of magnitudes. Hence the widths have a logarithmic growth and can be

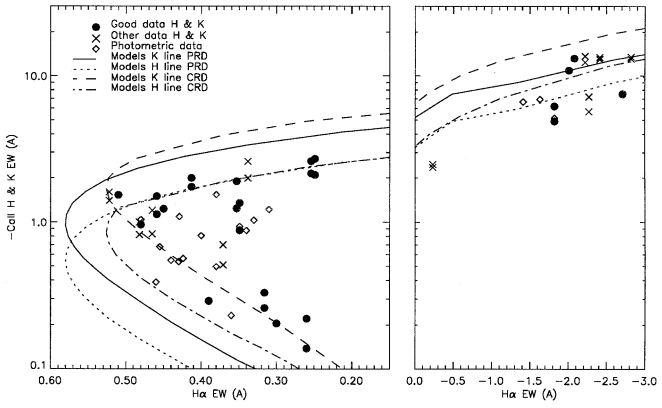

Fig. 11. CaII line equivalent widths as a function of H_α equivalent width for the models and the data. The large scatter in the data is attributed to surface inhomogeneities. The Calcium lines increase monotonically when H_α goes through the low, intermediate and high activity domains as illustrated by the models. Hence, for a given H_α equivalent width, the calcium lines can differentiate between the low and intermediate activity levels

approximated by the following formula (ignoring low accuracy measurements):

$$FWHM_{CaII} = 0.0878 \cdot log(-EW_{CaII}) + 0.216. \quad (4)$$

Given the present modelling approximations, radiation damping and changes in the chromospheric physical properties by themselves are not sufficient to reproduce the observed correlation. Precise measurements of rotational broadening for individual stars will have to be taken into account as well as a metallicity gradient and perhaps also a turbulence gradient (as a function of activity level) for the models. We find that a low calcium abundance will be necessary to reproduce the particularly narrow profiles at low activity levels.

5.5. H_α and Ca II lines

We plot in Fig. 11 the calcium line equivalent widths as a function of H_α equivalent width for the observations and the models. In a similar manner as the FWHM vs. EW diagram for H_α (Fig. 4), the Ca II equivalent widths increase monotonically as the H_α equivalent width reaches a maximum (absorption) and as H_α fills in. This feature shows that the calcium lines can be used to remove the near-degeneracy of the low activity and intermediate activity H_α profiles. For example, the profiles shown in Fig. 5a both have equivalent widths of about 0.26Å but there is an order of magnitude difference in the corresponding Ca II line equivalent widths (Fig. 11, right hand points in the left panel).

The observed and theoretical gradients for the Calcium line growth are both larger in the -0.1Å to -1Å domain (low activity) than in the -1Å to -3Å domain (intermediate activity). According to our calculations, this is evidence that the former domain corresponds to larger changes in chromospheric pressures, or in other words, that the intermediate activity domain takes place over a smaller pressure range (in a logarithmic scale) than the low activity domain. This of course is reminiscent of the rapid change in H_α from strong absorption to strong emission (Sect. 5.1).

Once again, models define an envelope to observations. They qualitatively agree with observations, but as in some previous figures, there remain important quantitative disagreements that indicate the importance of some as yet unidentified parameters. In the H_α emission domain, Series (c) models agree better with observations than Series (a) models, whereas the opposite applies in the H_α absorption domain.

Fig. 12 represents the calcium line widths as a function of the H_α equivalent width. According to the previous findings (Figs. 4, 10 & 11), the widths should display a behaviour similar to that of the equivalent widths (Fig. 11). Unfortunately, uncertainties are too large in our data to confirm this. Nevertheless, one can see a large increase in Ca II width with the H_α EW (left panel, circles) that most likely corresponds to the low activity domain. As outlined above, this probably reveals the effect of metallicity on the calcium lines (directly through the line formation and indirectly as an effect of metallicity on activity level, Sect. 7). In the high activity domain (right panel), the calcium line widths tend to increase with the H_α EW, whereas models predict a rather constant width. We believe that this is the signature of rotational broadening and perhaps also of increasing turbulence.

For a further evaluation of our models, we plot the Ca II line widths as a function of the H_α line width in Fig. 13. The expected variations are illustrated by the models, i.e., both widths first increase (left panel), but due to the slight fall in the H_α width at intermediate activity levels (Fig. 4b), the curve first reverses before rising again and eventually reaching the H_α emission domain. Some models indicate that at high activity levels the Ca II widths may start decreasing while the H_α width still increases. If, according to Sects. 5.1 to 5.3, high pressure plages are present on the stellar surface, such an effect might become detectable if its amplitude is large enough. In our present sample we have only few data points, but they are suggestive that such a trend might be present.

6. Broad-band colors, activity level and metallicity

In Paper V we discussed the formation of the UV continuum excess in M1 dwarf chromospheres and briefly compared those results with broad-band photometric observations. The comparison was extended to pre main-sequence stars and common characteristics were found. Here, we re-analyse in more detail these color-activity relations with a substantially augmented data set including the best available photometric measurements, and compare these data with model calculations.

We used Hα and the Ca II lines as complementary diagnostics, because they probe, respectively, the upper and lower layers of the chromosphere. In addition, the calcium lines vary monotonically with activity whereas the Balmer lines vary in a more complex manner but allow one to distinguish between two possibly distinct populations - the dM and the dMe stars. Moreover, the calcium lines are directly affected by metallicity

Table 3. Parameters of the least square fits to the empirical correlations (see text). We also give the χ^2 values, the number of points for those correlations and the type of stars to which they apply (dM(e) is for filled in profiles - intermediate activity)

Correlation	±	Star type	χ^2	n
$FWHM_{H\alpha}$ = 0.76$EW_{H\alpha}$ + 0.40	0.08Å	dM	1.9E-3	76
$SR_{H\alpha}$ = 0.67/(0.35 − $EW_{H\alpha}$) − 0.15	2EW	dMe & dM(e)	0.17	16
$log(-EW_K)$ = 0.921 $log(-EW_H)$ + 0.118	0.2EW	dM & dMe	1.8E-3	19
$FWHM_K$ = 0.846 $FWHM_H$ + 0.064	0.03Å	dM	3.7E-4	11
$FWHM_{CaII}$ = 0.0878 $log(-EW_{CaII})$ + 0.216	0.05Å	dM & dMe	9.7E-4	12
$U-B$ = 0.0410 $EW_{H\alpha}$ + 1.163	0.05mag	dMe	9.9E-4	20
$B-V$ = −0.186 $EW_{H\alpha}$ + 1.556	0.07mag	dM	1.6E-3	95
$U-B$ = 0.484 $(B-V)$ + 0.440	0.15mag	dM & dMe	3.7E-3	52
$B-V$ = −0.0148 $log(EW_{CaII})$ + 1.489	0.15mag	dM & dMe	5.3E-4	44
$B-V$ = −0.0135 $log(EW_{CaII})$ + 1.490	0.15mag	dM	4.6E-4	34
$FWHM_{H\alpha}$ = −0.0743M_v + 1.409	0.1Å	dM	3.6E-3	51
$FWHM_{H\alpha}$ = −0.0948M_v + 2.260	0.05Å	dMe	1.1E-3	7
$log(-EW_{CaII})$ = −1.090Mv + 10.66	0.25	dM & dMe	1.3E-2	8
$(log(-EW_{CaII})$ = −0.648Mv + 6.18)	0.5	dM & dMe	3.8E-2	25
$FWHM_{CaII}$ = −0.0992Mv + 1.23	0.05Å	dM & dMe	1.4E-3	27
$log(Lx)$ = −1.47Mv + 41.56	0.5 mag	dM & dMe	0.77	7

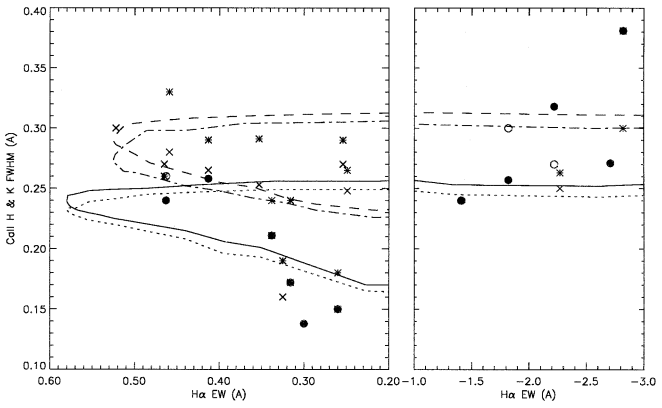

Fig. 12. CaII line FWHMs as a function of the H_α EW. Same description as Fig. 10. According to Figs. 10 and 11, the calcium line widths should display the same behaviour as their equivalent widths in Fig. 11, as illustrated by the model variations. The data suggest that pattern, but measurement errors are large. Models fail to reproduce the small widths at low activity levels

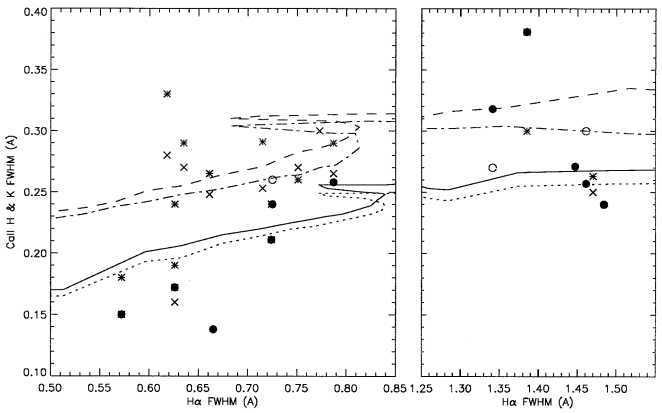

Fig. 13. CaII line FWHMs as a function of the H_α FWHM. Same description as Fig. 10. Here the data should show variations as illustrated by our models. When H_α is in absorption, the best data (circles) show a significant increase that we believe corresponds to the low activity domain while the points scattered in the upper part of the diagram correspond to the intermediate activity domain (indicated by the sharp left excursion of the theoretical curves)

but not the Hα line. The results are described separately for the two spectral lines and are interpreted and compared with models in a common subsection.

6.1. With the H_α diagnostic

We divided the H_α data set into three sub-samples: (i) our own measurements, (ii) other high resolution measurements, and (iii) narrow band photometric measurements (Herbst & Layden 1987; Herbst & Miller 1989). Broad band colors were taken in priority from the Hipparcos Input Catalogue (Turon et al. 1992) and from Legget (1992). Other sources were also used and averaged where applicable: Eggen (1974), Upgren & Lu (1986), Bessel (1990), Weis (1991ab, 1993), Gliese (1991).

When more than one H_α measurement was available for a given star, values were averaged. We found that the uncertainty arising from the variable character of the atmosphere is usually larger than the measurement uncertainty. For instance, Gl 15A was observed to have equivalent widths of: 0.316, 0.45, 0.33, 0.28 and 0.34. For Gl 411, we have 0.260, 0.36, 0.28 and 0.40 and for Gl 908, which we observed twice, we have 0.360, 0.380,

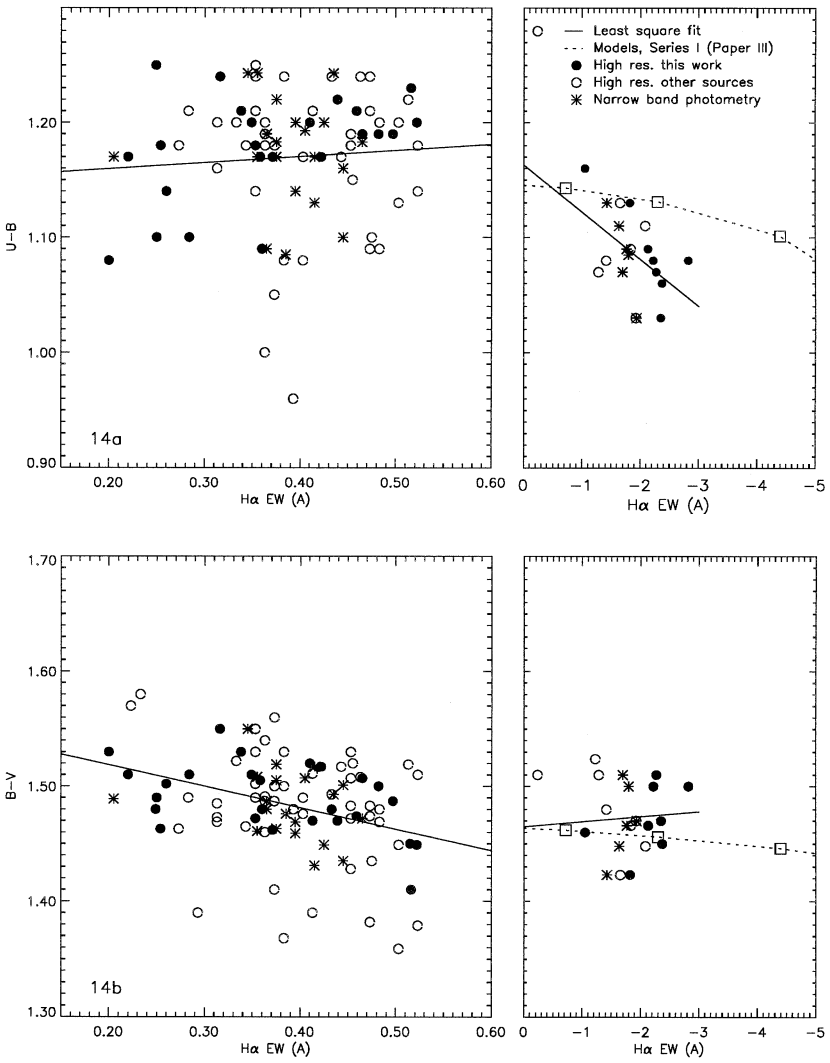

Fig. 14a–d. Broad-band U-B, B-V colors versus Hα and CaII equivalent widths. Note that the two sets of diagrams use different symbol descriptions. We observe a blue/UV excess for dMe stars (Hα in emission and large CaII equivalent widths). The large scatter in U-B in the Hα absorption domain and at low values of the CaII equivalent width is a metallicity effect. B-V diminishes only slightly, but this trend may be due to a surface structure activity, as one would expect the opposite trend from considerations on the stellar metallicities (see text). For comparison, we superimposed the model values (squares) in the emission domain

0.48, 0.40 and 0.36. Emission line stars are also known to be quite variable.

We plot the U-B and B-V colors against the Hα equivalent widths in Fig. 14. Each parameter is plotted into two subdiagrams for Hα in emission and absorption, as in Fig. 4. U-B is smaller on average for active emission line stars than for less active absorption line stars. The latter stars define a band, U-B$\in$[1.08:1.26], centered at 1.175 when we exclude the three stars with abnormally low colors, possibly due to flares, very low metallicities or incorrect measurements. As far as metallicity is concerned, we found that all dM stars with U-B$\leq$1.10 are halo or old disk stars, an indication that metallicity acts upon the ultra-violet flux.

Emission line stars have bluer colors and there may also be a correlation between the U-B excess and the strength of the Hα emission within the dMe stellar sample (Table 3 & Fig. 14a):

$$(U-B)_J \simeq 0.041\ EW_{H\alpha} + 1.163. \quad (5)$$

The data point in the upper left corner of the U-B figure for the emission domain represents Gl 140A. This abnormally large color confirms previous work showing that this star is a spectral binary with a cooler component. Excluding this star, we obtain <U-B>=1.089 for dMe stars, i.e. a 0.086 magnitude difference with dM stars on average, which is evidence for a U-band excess.

In B-V, there is a decreasing trend for dM stars (Fig. 14b): in the following equivalent width domains [0.20:0.31],]0.31:0.42[and]0.42:0.53] we find average colors of respectively 1.496$\pm$0.006, 1.488$\pm$0.0016 and 1.469$\pm$0.002. The average for dMe stars, 1.471, is very close to the value found when Hα is strongly in absorption. The difference of 0.027 magnitudes between lower and higher activity stars is at least 5 times larger than the uncertainties on the mean values.

When the Balmer lines are in absorption, the V band can be considered as free from spectral line contamination and the only possible contributor to the B-band is the Ca II doublet. Nevertheless, according to their fluxes in this activity range, their contribution is negligible and the possibility of spectral line contamination must be ruled out.

A similar trend is seen in R-I which suggests that our dM star sample is slightly biased as a function of the effective temperature: in R-I, the means are 0.872$\pm$0.001 and 0.880$\pm$0.005

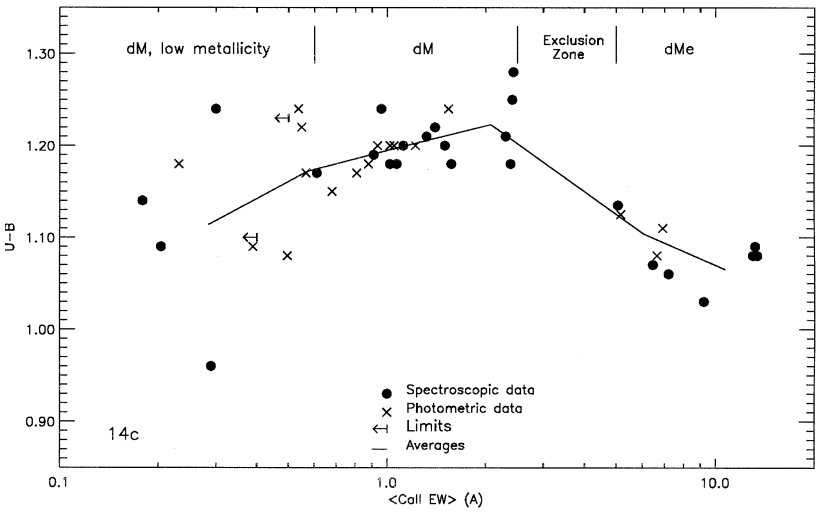

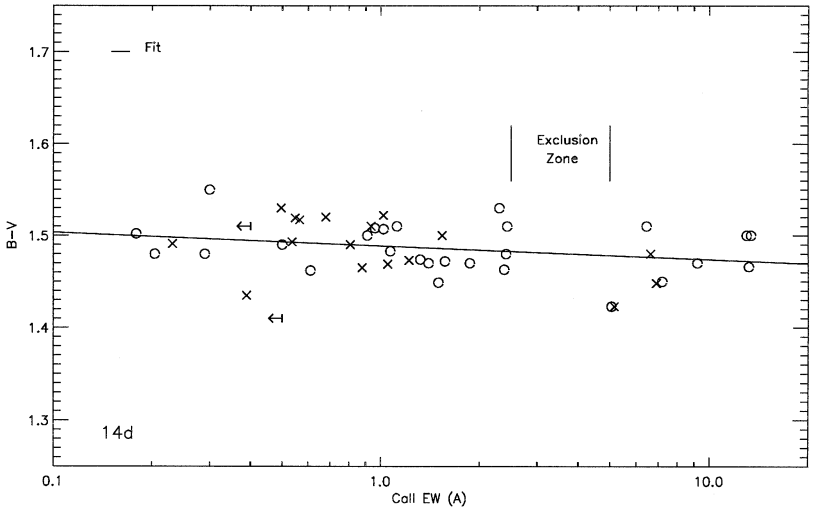

Fig. 14a–d. Continued

respectively for dM and dMe stars. Hence there is a slight difference in temperature between the dM and dMe sub-samples; according to Eq. (14) and Jones et al. (1994), dMe stars in our sample have on average a higher effective temperature by 5 K. This bias has no or very little effect on B-V and U-B, as these colors lose their temperature sensitivity for M dwarfs (Ryan 1989).

The scatter in U-B is about 0.18 magnitudes (9%) with dMe stars excluded, whereas in B-V most measures lie within a 0.13 magnitude band (6%) and in R-I it is constrained to a 0.12 magnitude band (5.7%). When we include dMe stars, these figures are 0.23 (11%), 0.18 (9%) and 0.12 (5.7%) respectively. These values are larger than measurement uncertainties and show that both metallicity (e.g. Buser & Fenkart 1990; Buser & Kurucz 1992) and/or magnetic activity (Fig. 14a) influence broad band fluxes, with an increasing effect towards shorter wavelengths for both the dM and dMe stellar sets.

6.2. With the Ca II diagnostics

We show the stellar colors as a function of the average Ca II line equivalent width in Figs. 14c and 14d. As in the case of the Hα line, we observe that B-V decreases when "magnetic activity", as seen in the Ca II lines, increases. The least square fit to the data yields;

$$(B-V)_J \simeq -0.0148\ log(EW_{CaII}) + 1.489. \quad (6)$$

This gives a 0.027 magnitude decrease in the observed equivalent width domain. Conversely, R-I increases slightly (0.011 magnitudes) for the same stellar sample. These trends may appear to conflict with the previous results obtained with Hα, but they do in fact confirm them: in the Ca II sample, we took into account simultaneously both the dM and dMe stellar sub-samples, but when taken separately these subsamples give results similar to that of the Hα sample; B-V and R-I diminish for dM stars when the line equivalent widths increase. When taking dM stars alone, the above correlation is almost unchanged (coefficients of -0.0135 and 1.490) but R-I remains constant (less than 2 m mag change).

According to B-V vs. R-I color diagrams (Ryan 1989), M1 dwarfs follow the empirical relation;

$$(B-V)_J = 0.37\ (R-I)_K + 1.15. \quad (7)$$

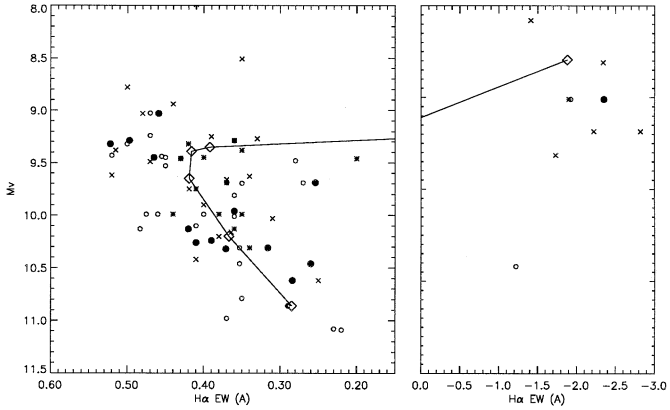

Fig. 15. Visual absolute magnitude against Hα equivalent width. Same description as in Fig. 14a, except that here crosses are for stars with a parallax uncertainty larger than 10%. We overplot the average values in six activity bands (continuous line, see text). According to the H_α equivalent width as an activity diagnostic (Fig. 4), surface activity increases with absolute magnitude (i.e., with the radius) for the stars in our sample (see also Fig. 17). This larger stellar sample is evidence that intermediate and high activity stars are outnumbered by low activity stars (see text). This diagram also shows that single dMe stars are on average 1.4 magnitudes brighter than single dM stars

This implies that for the observed variation in R-I, the corresponding variation in B-V is about three times smaller (note that the combination of empirical laws given by Pettersen (1983) and Legget (1992) yield an over-estimated gradient of 0.515), i.e. for dM stars the change in B-V should be no more than $\sim$2 millimag, when we observe a 15 millimag decrease for dM stars and 27 millimag when dMe stars are included. Although these variations are small, they are an order of magnitude larger than expected for a purely temperature effect. We shall see below that stars in our sample follow activity-luminosity relationships, which appear to show the effect of metallicity upon the stellar structure (Vandenberg et al. 1983): these are therefore activity-metallicity relationships.

Surface activity increases with metallicity (see also the discussion on Fig. 14c below), and with reference to metallicity-color calculations (Buser & Kurucz 1992), a depletion in metallicity should induce a B-V excess towards low activity stars. But the opposite is actually observed: low activity/low metallicity dM stars have a larger B-V than higher activity stars. We are therefore forced to conclude that there is another important atmospheric parameter at work, surface gravity or magnetic activity (Paper V). Surface gravity itself depends on metallicity but in the present case its effects should remain very small on the B-V color; probably less than 0.005 mag according to Buser & Kurucz (1992) calculations. The remaining principal agent is therefore magnetic activity, and the observations agree with the variations predicted by the models (see below and Paper V). Moreover, the continuity in the trend between the dM and dMe populations supports this argument, in particular if one considers that dMe stars are mixed old disk binaries and young disk stars.

The U-B vs. Ca II diagram shows a totally different picture (Fig. 14c): (i) at low activity levels (EW>-0.7Å), the scatter is very large and seems to increase towards lower levels, (ii) at normal and intermediate activity levels (-0.7Å>EW>-3Å), the scatter is small and comparable to that in other color indices (e.g., B-V in Fig. 14d), (iii) at high activity levels (EW<-3Å), U-B decreases sharply but the scatter is comparable to that at intermediate levels. We superimposed the measurements averaged over six intervals (-0.4Å: -0.7Å: -1.5Å: -3Å: -7Å). As already seen with the Hα line, dMe stars show an ultraviolet excess emission. Taking the normal metallicity disc stars (corresponding to normal and intermediate activity levels, Fig. 14c) as reference ([-0.7Å:-3Å] domain), this excess amounts to 0.119 magnitudes in average and can be as large as 0.26 magnitudes (a U-B value as low as 0.95 was observed for AU Mic).

For dM stars, U-B increases with the Ca II equivalent width, i.e., weak calcium emission stars exhibit an ultraviolet excess. On average, U-B increases monotonically with the calcium line strength, from 1.114 to 1.223, and in the case of Gl 1, a low metallicity Halo star, it is as small as 0.95. Before commenting further on those results, let us compare observations with the theoretical results exposed in Paper V.

6.3. Comparison with models and interpretation

A conclusive result on the comparison of observed colors with model calculations will have to await improved calculations because at present we use incomplete opacities and line blanketing. Ultraviolet line blanketing (e.g. Buser & Kurucz 1992) and molecular opacities (e.g. Allard et al. 1994) in cool dwarfs are problems that require extensive data compilations that have not been yet considered in such chromospheric modelling studies. Nevertheless, our models describe qualitatively the influence of the main b-f and f-f processes on the UV and visible continua which it is worth comparing with this observational set. Hence, we compare observations with differences between model colors rather than to the colors themselves.

In Paper III we considered two series of model chromospheres with a high and a low temperature minimum; respectively Series I and II. There is a 0.021 magnitude difference in U-B between these two series. Hence, the increase in the temperature minimum actually decreases the U-B color (increases the UV continuum). This is in agreement with the observations. We renormalised the model colors to the U-B value of 1.176 for our Series II and calculated the difference with Hα emission models in Series I. We overplotted the results in Fig. 14a. The changes in U-B color are significantly smaller for our models.

The models did not include the Ca II line contributions to the U, B and V bands, but according to our observations, the U-B excess has been underestimated by no more than 15% to 30%. We also found that the calcium lines largely dominate the line contamination to the U-band for H_α equivalent widths down to -5Å, but for stronger Balmer emission the calcium contribution falls to about 25% and the Balmer lines then dominate. The maximum spectral line contribution to the U-B excess is about 50%, which occurs for H_α equivalent widths of about -10Å.

Therefore, the observed UV excess is presently much larger than that produced by a chromosphere which matches the Hα and Calcium fluxes. To reproduce both the line equivalent widths and the UV excess, one must consider, as in the previous sections, higher pressure plages with a maximum filling factor of 40% (with reference to these models).

With our models, the effect of the temperature minimum on B-V is about 0.02 magnitudes and reaches 0.037 magnitudes when the chromosphere (models I-3 - II-5) is taken into account in the H_α emission domain. This is of the order of the detected decrease in B-V.

Observations confirm the predicted U-B excess for dMe stars and also suggest a slight B-V excess. The UV excess is on average a factor of 3 larger than predicted and in some instances a factor of 6 larger. This has important implications for the radiative energy budget of the outer atmosphere which should then be dominated by the UV continuum emission (Paper V) and points to possible high pressure "hot spots" on the stellar surface.

Another possible contribution to this excess may arise from a surface gravity effect (a metallicity effect is in principle excluded for dMe stars): for a dM and a dMe star of given mass, a factor of two difference in radius (see Sect. 8) yields a factor of 4 difference in surface gravity, but decreasing the surface gravity tends to deplete the H_α emission (Panagi 1990). Consequently, a higher chromospheric column mass is required to drive H_α into emission in a dMe star than is predicted by the present models. Another consequence of a smaller surface gravity is an increase in the photospheric UV intensity: according to Buser & Kurucz (1992) one can expect a decrease in U-B of $\sim$0.1 mag. for M0 dwarfs. These two effects combined may be sufficient to account for a supplementary U-B excess. The single, large radius dMe stars in our sample (St 497, Gl 803 and Gl 616.2, see Sect. 8) indeed are located in the lower part of the dMe group in Fig. 14a, with an average U-B=1.057 smaller by 0.032 mag. It would be interesting in future studies to look for such surface gravity effects in dMe stars. Surface gravity does not seem to play a role on the B-V correlation (previous subsection), however, as single dMe stars mix well with other stars in our sample.

With our conclusion that the UV excess for dMe stars depends mainly on surface activity, let us now consider the variations observed for the less active dM stars. It has long been established that metallicity is related to the ultraviolet excess of main-sequence and evolved stars (e.g., Sandage 1969; Carney 1979; Ryan 1989; Buser & Fenkart 1990; Buser & Kurucz 1992), and this UV excess is often used for metallicity calibration. With a small sample of stars and a somewhat large range in spectral type, Hartwick (1977) found a blue excess up to several tenths of magnitude that correlates with absolute magnitude for M dwarfs: brighter and more active stars exhibit a blue excess, whereas fainter subdwarfs show blue deficiencies. Hartwick concluded that the photometric UV excess can be used as a metallicity indicator, as proposed earlier by Sandage (1969) for hotter stars. Accordingly, we looked for correlations between the (U-B) and (B-V) colors with Mv but found none. So far we have no explanation for this lack of correlation because M dwarf luminosity should depend directly on metallicity (e.g., Vandenberg et al. 1983), but alike dMe stars, another mechanism acting on the stellar size may be involved (see Sect. 9). On the other hand, we found a weak correlation between these two colors (Table 3), indicating that some excess appears simultaneously in both the U and B bands.

As in other stars, the large variations in U-B for dM stars are most likely due to metallicity, and this effect probably increases with spectral type (Buser & Fenkart 1990; Buser & Kurucz 1992). We therefore interpret the large U-B scatter for M dwarfs as the signature of a metallicity effect (Fig. 14c). According to the low dependance of U-B and B-V as a function of R-I for M dwarfs, the [0.82:0.93] R-I domain should yield very constrained B-V and U-B domains. We interpret the large scatter and increasing average U-B color (Fig. 14c) as a metallicity effect.

One could argue that the low calcium fluxes in low metallicity stars are due entirely to lower calcium abundances, but the Hα vs. calcium relation (Fig. 11), shows that they are also connected to the activity level because Hα is not directly dependant on metallicity. Along the same lines, the luminosity vs. activity correlations (Sect. 7 and 9) tend to favor a dependence of the stellar size and/or metallicity on the activity level. We therefore conclude that the average trend depicted in Fig. 14c for dM stars is evidence that both U-B and magnetic activity rise with metallicity.

In conclusion, a U-B excess due to magnetic activity was detected for dMe stars with a maximum spectral line contamination of 50%. A possible B-V excess was also noted. A slight bias was detected in the R-I distribution versus H_α in our stellar sample, which, according to the activity-luminosity relationship discussed below probably reflects the increase in H_α with luminosity along the main-sequence (luminosity and H_α absorption strength both decrease with R-I). This small effective temperature effect should not, however, bias the B-V nor the U-B sample. We found that our models agree qualitatively with the observed trends even though they cannot yet match the observed amplitude. This result is consistent with the spectral line analysis and points to plage areas with a filling factor of about 30%.

7. Magnetic activity and stellar radius and metallicity: a new constraint on the dynamo mechanism?

7.1. H_α

We saw in Paper V that dMe stars are on average abnormally luminous when compared with the less active dM stars. Fig. 15 shows the absolute visual magnitude against the Hα equivalent width. Unfortunately, absolute magnitudes rely heavily on parallaxes which generally are poorly known even for nearby dwarfs: a 20% uncertainty corresponds to $\pm$0.40 magnitudes. Hence, we separated the measurements into two classes: those with parallaxes known to better than 10%, and those worse than 10%.

The M1 dwarfs we selected cover a rather large range in absolute visual magnitude, 2.9 magnitudes from 11.1 to 8.2, which means a factor of 14.5 in disc area and a factor of 3.8 in radius. A three magnitude scatter near the main sequence is expected for M dwarfs just from a metallicity effect (e.g., VandenBerg et al. 1983).

If one wants to estimate the influence of the stellar internal structure on the activity level, binary systems should be excluded because of their more complex properties and different angular momentum evolution. In our dMe stellar sample, only St 497, GJ 1264, Gl 616.2, Gl 781 and Gl 903 are probably single stars, but parallaxes are known only for Gl 616.2 and Gl 803. Their average absolute magnitude is $< M_v >= 8.59$, i.e. 1.4 magnitudes above that of dM stars ($< M_v >= 9.95$). The very few active stars used in our analysis means there is a large uncertainty on their average luminosity, nevertheless the large difference remains somewhat puzzling, especially since no lower activity dM stars with well known parallaxes are more luminous than the ninth magnitude. The higher luminosity of hydrogen emission line stars at M spectral types was also noted for instance by Veeder (1974) and by Stauffer & Hartmann (1986); in their samples, dMe stars were on average brighter by respectively $\sim$0.3 and $\sim$0.34 magnitudes.

We found a similar trend in the dM stellar sample: the H_α equivalent width seems to increase with luminosity and low luminosity stars all exhibit a weak H_α line (Fig. 15). Because intermediate activity stars (filled in H_α) also have a weak H_α equivalent width, they should be significantly more luminous than their low activity counterparts if there is a real trend. We checked this assertion on the basis of the calcium line measurements. We selected five activity domains according to the calcium line EW: very high (dMe) ≤ -3Å, high [-1.5;-3]Å, normal/high [-1;-1.5[Å, normal/low [-0.4;-1[Å and low >-0.4Å. We then averaged the corresponding H_α and Mv measurements and plot them in Fig. 15. The resulting curve, like those in preceding figures, shows that on average absolute magnitude decreases with the chromospheric pressure (and thus activity level) as diagnosed by the H_α line. On account of this variation, we chose a sixth band by assuming that very low luminosity stars (Mv$\geq$10.5), for which we have no Ca II measures, are all very low activity stars and there cannot be any contamination from intermediate activity stars in this domain. Averaged values in this band are consistent with those in the other bands, further strengthening the preceding explanation. Therefore, although the scatter in this diagram is very large, both because of uncertainties in absolute magnitudes and the complex variations of the H_α line, average values clearly indicate that surface magnetic activity increases with the stellar luminosity.

In this larger stellar sample, intermediate activity stars seem much less numerous than low activity stars, contrary to the proportions suggested by the Ca II vs. H_α measurements (due to the observational bias towards brighter stars for calcium; Fig. 11), and probably represent no more than 25% of the stellar population. This conclusion should also apply to the stellar unbiased population, because if there is any bias in our larger Mv vs. H_α sample, it should also be towards the more luminous stars, i.e., the most active stars.

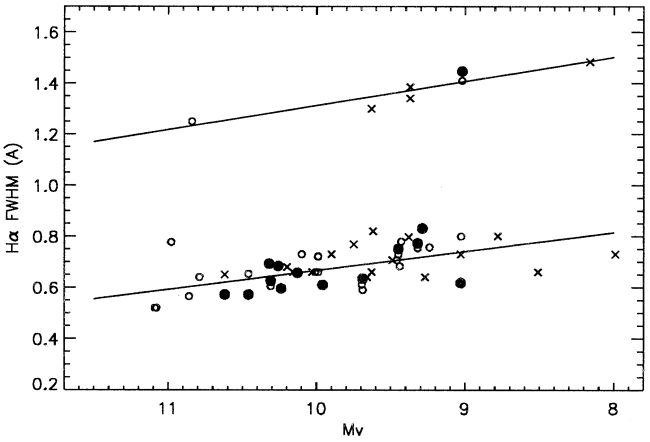

Fig. 16. Hα width as a function of absolute visual magnitude. Symbols are as in Fig. 15. In compliance with Figs. 4 and 15, we do obtain some correlation between these two parameters. According to Fig. 4, this Wilson-Bappu type of relationship emphasizes the changes in chromospheric properties with surface magnetic activity (Figs. 15 & 17)

In Fig. 16 we show the H_α FWHM as a function of absolute visual magnitude (Mv). As could be expected from Figs. 4 and 15, we also obtain a correlation between the two parameters for which a linear least square fit yields (see also Table 3),

$$FWHM_{H\alpha} = -0.0743 M_v + 1.409, \quad (8)$$

for dM stars. A similar correlation with a slightly larger slope is also found for dMe stars (Table 3). M dwarfs are slow rotators, and rotational broadening is unimportant. Instead, this correlation finds a simple explanation in the increasing activity level with luminosity (Figs. 15 & 17) combined with the increasing width with activity (Fig. 4). This Wilson-Bappu type of correlation may therefore principally reflect the changes in the chromospheric properties as a function of magnetic activity.

7.2. Ca II lines

As outlined above for the H_α line, the calcium lines also exhibit a correlation with luminosity, both for their equivalent widths (Fig. 17) and their FWHMs (Fig. 18). The linear fit to the accurate measurements in Fig. 17 yields;

$$EW_{CaII} = -exp[-1.090 M_v + 10.66], \quad (9)$$

where symbols take their usual meaning. Including all the data such as photometric measurements (with weights of 1 and 1/3 respectively for the best and least accurate data), the fit gives parameters of -0.648 and 6.18. In both fits binaries were not included. The fit obtained by Houdebine (1996) and which did not include Ca II photometric data gave a gradient of -0.909, rather close to our best data fit. Note that this preliminary result included all calcium line measurements, whereas here they were averaged for each star.

Because our stars all have the same spectral type, the stellar luminosity directly depends on the radius, and by substituting we obtain;

$$EW_{CaII} = aR_\star^{5.45}, \quad (10)$$

where $a = \frac{1.8410^{11}}{exp(0.91M_o)}[\frac{I_V}{F_o}]^{2.27}$, M_o and F_o are, respectively, the absolute visual magnitude and stellar flux for an apparent magnitude V=0, and I_V is the surface intensity in the V band for a star with $(R\text{-}I)_K$=0.88. For the same reason, the calcium line equivalent widths are proportional to the surface fluxes, providing that the differential effects of surface gravity and metallicity on the adjacent continuum intensity can be ignored in first approximation. In addition, one may consider that for dM stars, the total radiative losses in the outer atmosphere grossely scale as chromospheric line fluxes, e.g. the Ca II lines (Linsky 1991). For the time being, we can only apply the same assumption to dMe stars, although recent calculations suggest a differential growth in the main cooling agents (Paper V, see also Sect. 6). Since the absolute magnitude is proportional to $4.5\log R_\star$, and assuming that radiative losses are proportional to the non-thermal heating rate, using Eq. (10) we can relate the surface radiative losses to the stellar radius, $F_{Rad} \propto R_\star^{4.54}$. Considering that acoustic heating should be the main heating mechanism only for the least active stars and can be neglected for higher activity stars, we can then relate the total stellar magnetic flux to the stellar radius;

$$F_{mag} \propto R_\star^{7.45}. \quad (11)$$

At present, this relation should be regarded with some caution because of the unknowns in non-thermal heating mechanisms, but this result emphasizes *the importance of the stellar size (i.e., internal structure) on the efficiency of the dynamo mechanisms*. It is important to stress that the dependence on the radius is higher than on any other stellar parameter including the rotation rate, highlighting the importance of this new property for the magnetic activity problem. A large scatter in the diagram is implicit because the effects of rotation, metallicity and surface gravity have not been isolated here.

The Ca II line widths also show a dependence on stellar luminosity (Fig. 18). They increase by a factor of two over a 1.5 magnitude range and obey the relation,

$$FWHM = -0.0992Mv + 1.23. \quad (12)$$

We replace the absolute magnitude by its dependence on the stellar radius to obtain;

$$FWHM = 0.60log(R_\star) + A, \quad (13)$$

where $A = 0.30log(\frac{4\pi I_v}{F_o}) - 0.12M_o + 1.42$. The cause of this Wilson-Bappu type of relationship is not yet clear, but surface gravity, microturbulence, rotation and magnetic activity all probably play a significant role.

8. Field dMe stars: stellar spots, the last stage before the main-sequence or low metallicity?

We saw in the previous section that magnetic activity increases as the power of ∼7.5 of the stellar radius, and that active, single dMe stars stand largely above the mean of the dM stars in a color-luminosity diagram. Is this evidence that some active dwarfs have not yet reached the zero-age main sequence (ZAMS)? This problem has been the subject of some debate since Haro & Morgan (1953) discovered the so-called "flare stars" in the Orion association (see Mirzoyan 1993 for a review). Magnetic activity was subsequently showed to be systematically associated with youth notably in young stellar clusters, with the exception of the "extreme T Tauri stars" for which suspected signatures of magnetic activity are not as evident. Haro (1957, 1962) first suggested the pre-main sequence nature of active dwarfs in clusters as an intermediate class between T Tauris and the ZAMS. The discovery of such stars in the Hyades (e.g. Mirzoyan et al. 1989) and their spectral characteristics similar to those of active field dwarfs is evidence that for low mass stars this active state can be sustained for hundreds of millions of years.

The youth and pre-main sequence nature of some active dwarfs in young cluster is not contested, but, on the other hand, the evolutionary status of the nearby active dwarfs is rather puzzling. Among those stars we should distinguish between those that are active due to their binarity and the presumably single active stars. As many as 85% of the nearest active dwarfs are binaries (Evans 1977). However, when the star has no obvious companion and rotational broadening is detected (e.g. AD Leo and AU Mic), there are high chances that we are dealing with a single, relatively fast rotating star. In M dwarf binaries chances are high that stellar rotation axes and the system rotation axis are aligned. In our sample, we have two such examples - AU Mic and Gl 616.2. Both are far more luminous than their dM equivalents. Because evolutionary effects for stars with a mass below $0.6M_\odot$ are small or negligible (e.g. Vandenberg et al. 1983), either they have an abnormally high metallicity (Vandenberg et al. 1983) or they have not yet contracted to the main-sequence. In the light of their space motions and metallicity indicators,

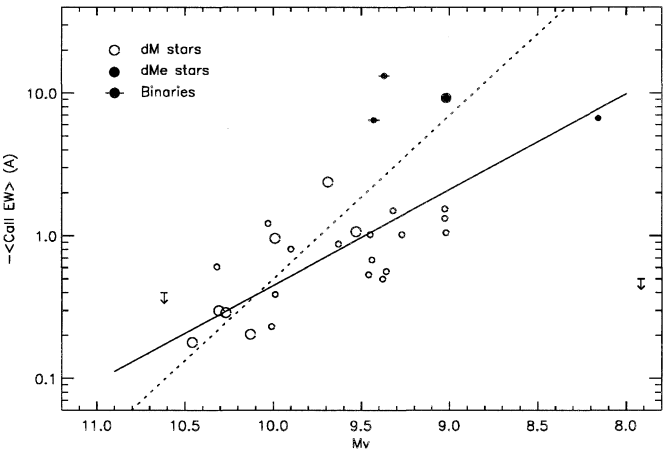

Fig. 17. Same diagram as Fig. 15 for the CaII lines. We also show the linear least square fit to the data that yields a dependence of the CaII line surface fluxes on the stellar radius to the power of 5.5. This is a strong indication that on average the stellar magnetic flux has a high dependence on the stellar radius (approximately as the power of 7.5): a decisive constraint for stellar dynamo and atmosphere theories

which are like other disk stars, we must turn towards the second option.

The recent spectral classification by Jones et al. (1994) provides one of the most accurate determination of the stellar effective temperature T_{eff} for M dwarfs. We plotted the (R-I)$_c$ color against the effective temperature for their template stars and found a good linear correlation:

$$T_{eff} \simeq -799(R-I)_c + 4372. \quad (14)$$

Gl 411 is in our selected sample and is also one of their template stars. We can therefore determine quite reliably some properties of our target stars by comparison with Gl 411. For this star we obtain R = 0.430$R_\odot$ and T_{eff} = 3461 K, the latter being recomputed with Eq. (14) for the sake of consistency. Then, for stars in our sample we find that the stellar radius is given by:

$$R = \frac{6.3710^7}{T_{eff}^2 \pi (exp(0.4 m_v))^{1/2}} R_\odot, \quad (15)$$

where π is the parallax and m_v the apparent visual magnitude. Knowing the effective temperature and radius we can compute the bolometric luminosity using the Stefan-Boltzmann law. We then compared these results with the evolutionary tracks of Vandenberg et al. (1983) and D'Antona & Mazzitelli (1985). We found the following values for AU Mic and Gl 616.2:

- AU Mic: 3485 K, $0.82R_\odot$, $8.9510^{-2}L_\odot$, $\sim 0.5M_\odot$, age$< 10^7 yr$
- Gl 616.2: 3653 K, $1.11R_\odot$, $0.198L_\odot$, $\sim 0.65M_\odot$, age$< 10^7 yr$

The stellar radii are much larger than those of non-active dwarfs and for Gl 616.2 it is even larger than for the Sun. The masses are rather model dependent and there is a disagreement of 0.1 $M_\odot$ or more between the Vandenberg et al. (1983) and D'Antona & Mazzitelli (1985) calculations. On the Vandenberg et al. (1983) evolution diagram, the two stars define the same isochrone with an age slightly below 10 million years. This result is totally inconsistent with the expected age of field dwarfs.

A large uncertainty remains in pre-main sequence evolutionary tracks, and observations of the Hyades show that magnetic activity for single dwarfs can last at least a few hundreds of millions of years. Are the evolutionary tracks wrong by an order of magnitude by predicting a contraction phase usually less than a hundred million years, or are these stars indeed very young?

Ambartsumian (1957) proposed that nearby UV Ceti-type dwarfs are part of a cluster that still exists, while Herbig (1962) suggested that they were formed in clusters that have scattered. Observations of the space density by Mirzoyan et al. (1988) showed that they are evenly scattered in the solar neighbourhood and therefore support the second alternative. However, the decay time for clusters is rather large and is incompatible with the young age of the previous stars as suggested by their high luminosity. Too little is understood so far to draw any firm conclusion about the status of nearby active dwarfs, but their unusual luminosities are a strong argument in favor of their possible pre-main sequence nature, and yet another indication of their youth (Mirzoyan et al. 1989).

Gl 781 also exhibits H$_\alpha$ in emission but unlike Gl 803 and Gl 616.2, it is a subluminous halo dwarf located 1.30 magnitudes below the main-sequence (Stauffer & Hartmann 1986, Legget 1992). This star, however, has a high projected rotational velocity of 15 km s^{-1} and is probably a binary according to Stauffer & Hartmann (1986). In their stellar dMe sample, two other low metallicity stars are apparently single or in detached systems and have undetected rotational velocities - Gl 15B and Gl 812A. Both seem to have low metallicities, old disk motions, and Gl 15B lies 1 mag below the main sequence. This conflicts with the preceding comment that single dMe stars may be pre-main sequence stars. In young stars, there is well established evidence that contrary to theoretical predictions, some stars free of diffuse circumstellar absorption do indeed lie below the main sequence (Haro 1988) and in fact show a large scatter about the ZAMS (e.g. Haro & Chavira 1966, Natsvlishvili 1990, Mirzoyan 1993). This could be a signature of large spot coverage (see below), but this should not apply for older disk and halo stars. Instead, we propose an alternative explanation for the *apparent* high activity level of single halo dwarfs.

Observations of gravity-sensitive indices (Mould & Hyland 1976, Stauffer & Hartmann 1986) show that surface gravity increases substantially when metallicity decreases. Preliminary calculations of the effect of gravity on the H$_\alpha$ line (Panagi 1990) showed that it goes into emission for a much smaller column mass in the transition region than for normal surface gravity stars. Moreover, the depletion in metallicity, typically a factor of 10 according to Mould (1976), will probably change the relative contribution of the chromospheric cooling agents. Radiative cooling in metal lines (e.g. Ca II and Mg II) will become weaker and for a given non-thermal heating rate, the chromospheric pressure must increase to compensate because the formation of these lines is collisionally controlled. This change in the chromospheric energy balance may be sufficient, if not to drive H$_\alpha$ in emission in most low metallicity stars, at least to lower considerably the activity threshold above which H$_\alpha$ is in emission. In other words, *there may exist low activity/low metallicity dMe stars*, and more generally, *H_α is indirectly dependant on metallicity*.

It was also suggested that the large spot coverage of active dwarfs could alter their position in the H-R diagram. However, theoretical calculations of the Zero-Age Main Sequence for spotted stars (e.g. Spruit & Weiss 1986) show that active M dwarfs should be subluminous, but by no more than about 0.3 magnitudes. On the other hand, the apparent continuity in magnetic activity level as a function of absolute magnitude (Figs. 15 & 17) between the dM and dMe stellar populations suggests that there is no real dichotomy, and that some dM stars are nearly as active as dMe stars. Therefore, H$_\alpha$ emission is not as a peculiar characteristic as it may have been believed. In addition, some luminosity differences cannot be attributed to metallicity nor evolution. Consequently, there is a luminosity and activity versus metallicity paradox: unless M1e dwarfs and perhaps also some intermediate activity M1 dwarfs have not yet reached the ZAMS, stellar interior models still must explain important luminosity differences between M dwarfs.

9. The dynamo mechanism versus stellar internal structure

The continuity between the dM and dMe stellar populations, suggested by the stellar activity-radius correlations in Figs. 15 and 17, points to an interesting property relating the stellar interior to its magnetic dynamo. Early investigations of other magnetic activity indicators such as the X-ray luminosity L_X have shown unanimously that they correlate with the projected rotational velocity $v \sin i$ or the Rossby number (R_o) (e.g. Pallavicini et al. 1981, Mangeney & Praderie 1983, Fleming et al. 1989). As for the dependence on stellar size, such as the one found here, there are contradictory results. For instance, Fleming et al. (1989) found that $L_X \propto (v \sin i)^{1.05 \pm 0.08}$, but because L_X does not correlate with $\Omega \sin i$, then the previous correlation is with the stellar radius rather than the rotation rate. They found indeed a strong correlation with radius and that approximately $L_X \propto R_\star^2 \propto M_\star^2$. They postulate, however, that this correlation is induced by an observational selection effect towards the most active stars and that this correlation represents an upper boundary in L_X.

Similarly, Pettersen (1989b) found that flare activity in dMe stars is directly proportional to the volume of the convection zone. He also obtained a similar relationship with the X-ray luminosity for the same stars.

Curiously, these important findings were later disregarded. Other investigations focused on the dependence of X-ray luminosity with bolometric luminosity or absolute magnitude. Not surprisingly, it was found, in agreement with the Fleming et al. (1989) finding, that L_X decreases with L_{bol} or M_v. Such a correlation was shown later to be in fact an upper limit (or saturation) with a more complete sample by Barbera et al. (1993). This is not, however, evidence for a lack of dependence of the magnetic dynamo with the stellar radius. The problem with such analyses is that the effects of the four important stellar parameters, T_{eff}, $R_\star$, rotation and metallicity were never discriminated. For instance, at a given spectral type the bolometric magnitude spreads over three magnitudes, metallicity covers a large range and the rotation period spans from 10 h to several weeks. Hence for a given luminosity, spectral types are mixed and so are the variety of internal properties and dynamo mechanisms.

Here we take another approach by eliminating the effective temperature parameter. Among our program stars, 7 were detected with the Einstein Observatory Imaging Proportional Counter, and upper limits were obtained for another 4 (Barbera et al. 1993). We plot the X-ray luminosity (L_X) as a function of absolute visual magnitude in Fig. 19. We find the following correlation between the two parameters;

$$log(L_X) = -1.47 M_v + 41.56, \quad (16)$$

which when introducing the stellar radius yields,

$$L_X = k R_\star^{7.34} \quad (17)$$

where $k = \frac{3.93\ 10^{45}}{exp(1.47 M_o)} [\frac{I_\nu}{F_o}]^{3.67}$ and other parameters are as previously defined. This correlation supports the correlations found for the chromospheric line fluxes.

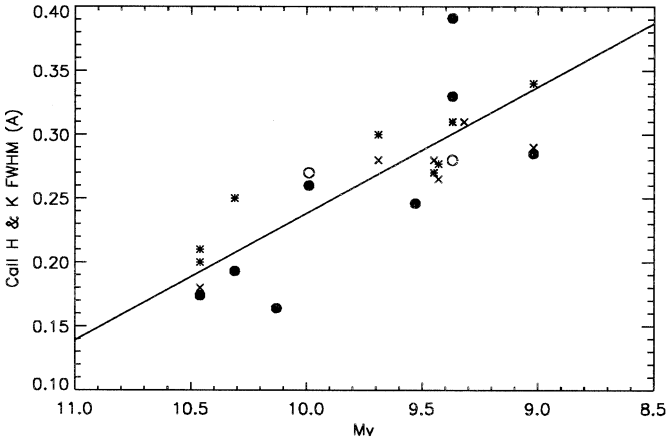

Fig. 18. Same diagram as Fig. 16 but for the CaII lines. This Wilson-Bappu type of relationship provides additional evidence that physical conditions in stellar atmospheres drastically change with the stellar size (Fig. 17), i.e., that optical depths, electron pressure and turbulence probably increase with magnetic activity

The increase in magnetic activity with stellar size overwhelms by far the effects of rotation. The latter is confined typically to an order of magnitude for chromospheric fluxes (Marilli et al. 1986), while the luminosity-activity correlation spreads over two orders of magnitude (Fig. 17). X-ray fluxes in our sample cover a range larger than three orders of magnitude, and we expect that it would reach four or more if our fainter program stars were detected.

All stars in our Ca II subsample (Fig. 17) are apparently old disk stars with the exception of the brightest Gl 803 (YD) and one of the faintests Gl 1 (Halo) (Legget 1992). Mould & Hyland (1976) and Mould (1978) showed that luminosity differences between the various component populations and even the rather large luminosity range for the old disk population alone can be explained by metallicity differences. This is in qualitative agreement with the VandenBerg et al. (1983) numerical simulations. But, as higlighted in the preceding section, metallicity alone cannot explain all luminosity differences, and many over-luminous dMe stars are known to have near solar metallicities (e.g. Taylor 1970, Hartmann & Anderson 1977, Naftilan & Fairchild 1993). Hence, these results lead one to believe that the radius-activity correlations are in fact the superimposition of two correlations: (i) one that could be referred to as a *metallicity-activity correlation* (stellar size increases with metallicity), and (ii), another that concerns stars with similar metallicities (mostly solar) but different radii and therefore activity levels, and is suggestive of an *age-activity correlation*. The former should concern the majority of main-sequence stars, whereas the latter includes the young active dwarfs which evolutionary status is thus far not clear. It is interesting that regardless of the parameter influencing the stellar size, all stars in our sample presently follow the same radius-activity correlation.

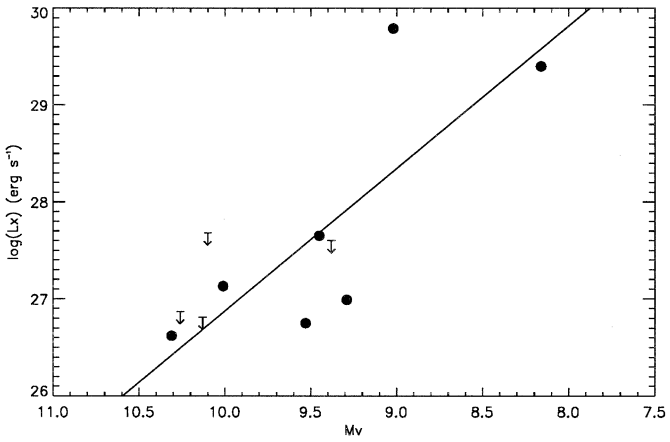

Fig. 19. X-ray luminosity as a function of absolute magnitude. The correlation between these two parameters confirms our finding that magnetic activity is highly dependent on the stellar radius. We overplot the linear least square fit to the data

10. Conclusion

In this study and in former papers in this series, we assessed some aspects of the complexity of stellar atmospheres by attempting to isolate the effects of one given stellar parameter at a time. The joint observational and numerical investigations prove to be a very powerful tool in this respect. As an example, within a narrow band near spectral type M1, we have studied the effects of magnetic activity, stellar size and metallicity on chromospheric spectral diagnostics and showed that they are interdependent. For dM1 stellar atmospheres, we have successfully reproduced the main properties of our numerical calculations for the hydrogen lines and also important characteristics of the Ca II resonance doublet. Our results provide evidence that finer atmospheric properties such as micro-turbulence can potentially be further constrained, and they give credit to investigations with one component model atmospheres in order to gauge these properties.

New empirical correlations between the spectral line characteristics have been identified that emphasize the importance of surface inhomogeneities and constrain essential properties of the atmosphere such as the transition region pressure, temperature minimum and velocity fields. A large variability was noted in H_α profiles even for rather low activity stars. The comparison of observations with models suggests that the column mass at the transition region ($log(M) \geq -5.5$) is higher for the vast majority of stars than for the sun. This currently implies that most M1 stars are far more active than the Sun.

We find that in our sample single dMe stars are on average more luminous than their dM counterparts. However, according to the activity-luminosity correlations there seems to be no dichotomy between the dM and dMe stellar populations. This questions the real physical mechanisms behind these correlations and the stellar internal structures, as well as the evolutionary status of dMe stars and perhaps also of "intermediate activity" stars.

We confirm an ultra-violet excess due to continuum emission in dMe stars that is about three times larger than expected from our model calculations. This, together with similar discrepancies found for spectral lines, all converge to conclude that with the present models high pressure plages are required with filling factors of the order of 30%.

We found additional Wilson-Bappu type correlations between spectral line characteristics and absolute visual magnitude, and thus with stellar size. For example, we show that both the H_α and Ca II line chromospheric diagnostics demonstrate an increase in radiative losses, and therefore non-thermal heating, with stellar size. More exactly, we found that the surface and total radiative losses in the calcium doublet increase, respectively, as the power of 5.5 and 7.5 of the stellar radius, providing an additional constraint for stellar atmosphere and dynamo theories. Hence, investigating the effects of the individual stellar parameters seems promising for future progress in understanding stellar dynamos.

Comparison of models with observations indicates that a complete treatment of molecular opacities and improved model atoms will be a necessary step in future NLTE calculations of chromospheric diagnostics. Although there is evidence for surface inhomogeneities, we show that one component model atmospheres can reproduce the integrated spectral signatures and help considerably understand the physics of stellar chromospheres.

Acknowledgements. This work was supported by a Research Fellowship at the ESA Space Science Department at ESTEC and as a visitor to the Sterrenkundig Instituut. We would like to thank the referee, J.L. Linsky, for improving both the content of this paper and Paper V in this series. We are particularly grateful to M. Carlsson and H. Uitenbroek for providing their respective version of the code MULTI and continued support. We would also like to acknowledge the benefit of using the Simbad database operated at CDS (Strasbourg, France).

References

Allard F., Hauschildt P.H., Miller S., Tennyson J., 1994, ApJ 426, L39
Allen C.W., 1973, Astrophysical Quantities, The Athlone Press, London
Ambartsumian V.A., 1857, in Variable Stars, ed. M.A. Arakelyan, Armenian Academy of Sciences, 9
Ayres T.R., 1979, ApJ 228, 509
Barbera M., Micela G., Sciortino S., Harnden Jr. F.R., Rosner R. 1993, ApJ 414, 846
Bessel M.S., 1990, A&AS 83, 357
Bopp B., 1987, ApJ 317, 781
Buser R., Fenkart R.P., 1990, A&A 239, 243
Buser R., Kurucz R.L., 1992, A&A 264, 557
Byrne P.B., Doyle J.G., Menzies J.W. 1985, MNRAS 214, 119
Carlsson M., 1992, Cool Stars, Stellar Systems and the Sun, ASPCS 26, 499
Carney B.W., 1979, ApJ 233, 211
Chang E.S., Avrett E.H., Loeser R., 1991, A&A 247, 580
Cram L.E., Giampapa M.S., 1987, ApJ 323, 316
Cram L.E., Mullan D.J., 1985, ApJ 294, 626
Cram L.E., Woods T.D., 1982, ApJ 257, 269

D'Antona F., Mazzitelli I., 1985, ApJ 296, 502
Derrider G., van Rensbergen W., 1976, A&AS 23, 147
Doyle J.G., Byrne P.B., Menzies J.W., 1986, MNRAS 220, 223
Doyle J.G., Houdebine E.R., Mathioudakis M., Panagi P.M., 1994, A&A 285, 233
Eggen O.J., 1974, PASP 86, 697
Evans D.S., 1977, in Flares Stars, ed. L.V. Mirzoyan, Armenian Academy of Sciences, Erevan, 40
Fleming T.A., Gioia I.M., Maccacaro T., 1989, ApJ 340, 1011
Fosbury R.A.E., 1973, A&A 27, 129
Giampapa M.S., Worden S.P., Schneeberger T.J., Cram L.E., 1981, ApJ 246, 502
Giampapa M.S., Worden S.P., Linsky J.L., 1982, ApJ 258, 740
Giovanardi C., Palla F., 1989, A&AS 77, 157
Giovanardi C., Natta A., Palla F., 1987, A&AS 70, 269
Gliese W., 1969, Catalogue of Nearby Stars, Veröff. Astron. Recher-Institut Heidelberg, No. 22
Gliese W., Jahreiss H., 1988, Astrophys. and Space Science 142, 49
Gliese W., 1991, preliminary version of the Third Catalogue of Nearby Stars, IDL Astronomical Library
Haro G., 1957, in Nonstable Stars, proceedings, ed. G.H. Herbig, Cambridge University Press, 25
Haro G., 1962, in Symposium on Stellar Evolution, ed. J. Sahade, Astron. Observ. Nat. Univ. La Platta, 37
Haro G., 1988, Astrophyzika 29, 18
Haro G., Chavira E., 1966, Vistas in Astronomy 8, 89
Haro G., Morgan W., 1953, ApJ 118, 16
Hartman L., Anderson C.M., 1977, ApJ 215, 188
Hartwick F.D.A., 1977, ApJ 214, 778
Herbig G., 1962, ApJ 135, 736
Herbst W., Layden A.C., 1987, AJ 94, 150
Herbst W., Miller J.R., 1989, AJ 97, 891
Houdebine E.R., 1990, PhD Thesis of Paris XI University at Orsay
Houdebine E.R., 1995, La Lettre de l'OHP, 14, 3
Houdebine E.R., 1996a, in Stellar Surface Structures, IAU Symp. 176, proceedings, ed. K.G. Strassmeier, in press
Houdebine E.R., 1996b, in Solar & Stellar Dynamos, proceedings, eds. J.F. Donati et al.
Houdebine E.R., Panagi P.M., 1990, A&A 231, 459
Houdebine E.R., Doyle J.G. 1994a, A&A 289, 169 (Paper I)
Houdebine E.R., Doyle J.G. 1994b, A&A 289, 185 (Paper II)
Houdebine E.R., Doyle J.G. 1995, A&A, in press (Paper IV)
Houdebine E.R., Butler C.J., Doyle J.G., 1993, Irish Astron. J. 21, 102
Houdebine E.R., Doyle J.G., Butler C.J., 1993, Irish Ast. J. 21, 102
Houdebine E.R., Doyle J.G., Kościelecki M., 1995, A&A 294, 773 (Paper III)
Houdebine E.R., Mathioudakis M., Doyle J.G., Foing B.H., 1996, A&A, 305, 209 (Paper V)
Janev et al., 1987, Elementary Processes in Hydrogen-Helium Plasmas
Jones H.R.A., Longmore A.J., Jameson R.F., Mountain C.M., 1994, MNRAS 267, 413
Judge P.G., 1990, ApJ 348, 279
Kelch W.L., Linsky J.L., Worden S.P., 1979, ApJ 229, 700
Lang K.R., 1980, Astrophysical Formulae, Springer-Verlag Press, Berlin
Legget S.K., 1992, ApJ 82, 351
Linsky J.L., 1991, Mechanisms of Chromospheric and Coronal Heating, eds. P. Ulmschneider, E.R. Priest & R. Rosner (Springer-Verlag), 166
Mangeney A., Praderie F., 1983, Active Phenomena in the Outer Atmosphere of the Sun and Stars, eds. J.C. Pecker & Y. Uchida
Marilli E., Catalano S., Trigilio C., 1986, A&A 167, 297
Mihalas D., 1967, ApJ 149, 169
Mihalas D., 1978, Stellar Atmospheres (Freeman & Co.)
Mirzoyan A.V., 1993, Astrophysics 36, 170
Mirzoyan L.V., Ambaryan V.V., Garibdzhanyan A.T., Mirzoyan A.L., 1988, Astrophysics 29, 430
Mirzoyan L.V., Ambaryan V.V., Garibdzhanyan A.T., Mirzoyan A.L., 1989, Astrophyzika 31, 259
Mould J.R., 1976, ApJ 207, 535
Mould J.R., 1978, ApJ 226, 923
Mould J.R., Hyland A.R., 1976, ApJ 208, 399
Mullan D.J., Cheng Q.Q., 1993, ApJ 412, 312
Naftilan S.A., Fairchild K., 1993, PASP 105, 565
Natsvlishvili R. Sh., 1990, Flare Stars in Star Clusters, Associations and the Solar Vicinity, eds. L.V. Mirzoyan, B.R. Pettersen & M.K. Tsvetkov, IAU Symp. 137, Kluwer Acad. Publish., 101
Pallavicini R., Golub L., Rosner R., Vaiana G.S., Ayres T., Linsky, J.L., 1981, ApJ 248, 279
Panagi P.M., 1990, PhD Thesis of Queen's University-Belfast
Panagi P.M., Byrne P.B., Houdebine E.R., 1991, A&AS 90, 437
Parker E.N., 1979, Cosmical Magnetic Fields (Clarendon Press, Oxford)
Pettersen B.R., 1983, Activity in Red-Dwarf Stars, IAU Coll. 71, 17
Pettersen B.R., 1989a, A&A 209, 279
Pettersen B.R., 1989b, Solar Phys. 121, 299
Pettersen B.R., Hawley S.L., 1989, A&A 217, 187
Priest E.R., 1982, Solar Magnetohydrodynamics (Reidel, Dordrecht)
Queloz D., 1994, internal publication of Observatoire de Haute Provence; "ELODIE, Programme de Réduction"
Roberts P.H., 1967, An Introduction to Magnetohydrodynamics (Longmans, London)
Robinson R.D., Cram L.E., Giampapa M.S., 1990, ApJS 74, 891
Rodonò M., 1986, The M-type stars, eds. R.J. Hollis & F.R. Querci, NASA SP-492
Rutten R.G.M., 1986, A&A 159, 291
Rutten R.G.M., Schrijver C.J., Zwaan C., Duncan D.K., Mewe R., 1989, A&A 219, 239
Ryan S.G., 1989, A.J. 98, 1693
Sandage A., 1969, ApJ 158, 1115
Schrijver C.J., Rutten R.G.M., 1987, A&A 177, 143
Schaifers K., Voigt H.H. (editors) 1982, Numerical Data and Functional Relationships in Science and Technology, Group VI, Vol. 2 (Springer-Verlag)
Seaton M.J., 1960, Report Prog. Phys. 23, 314
Simon T.D., 1992, Cool Stars, Stellar Systems and the Sun, ASPCS 26, 3
Spruit H.C., Weiss A., 1986, A&A 166, 167
Stauffer J.R., Hartman L.W., 1986, ApJS 61, 531
Stephenson C.B., 1986a, AJ 91, 144
Stephenson C.B., 1986b, AJ 92, 139
Sutton K., 1978, JQSRT 20, 333
Taylor B.J., 1970, ApJS 22, 177
Turon C., Creze M., Egret D. et al., 1992, ESA SP-1136
Upgren A.R., Lu P.K., 1986, AJ 92, 903
Uitenbroek H., 1989a, A&A 213, 360
Uitenbroek H., 1989b, A&A 216, 310
VandenBerg D.A., Hartwick F.D.A., Dawson P., Alexander D.R., 1983, ApJ 266, 747
Vaughan A.H., Preston G.W., 1980, PASP 92, 395
Veeder G.J., 1974, ApJ 79, 1056
Vernazza J.E., Avrett E.H., Loeser R., 1981, ApJS 45, 635

Vriens L., Smeets A.H.M., 1980, Phys. Rev. A22, 940
Vyssotsky A.N., 1943, ApJ 97, 381
Vyssotsky A.N., 1956, AJ 61, 201
Vyssotsky A.N., 1958, AJ 63, 77
Weis E.W., 1991a, AJ 101, 1882
Weis E.W., 1991b, AJ 102, 1795
Weis E.W., 1993, AJ 105, 1962
Wilson O.C., Vainu-Bappu M.K., 1957, ApJ 125, 661
Worden S.P., Schneeberger T.J., Giampapa M.S., 1981, ApJS 46, 159

This article was processed by the author using Springer-Verlag TEX A&A macro package version 3.